NASA CONTRACTOR REPORT

NASA CR-1410

NASA CR-1410

NASA CR-14

C. 1

INVESTIGATION OF THE TURBULENT WIND FIELD BELOW 150M ALTITUDE AT THE EASTERN TEST RANGE

by Alfred K. Blackadar, John A. Dutton,
H. A. Panofsky, and Anton Chaplin

NATIONAL AERONAUTICS AND SPACE ADMINISTRATION • WASHINGTON, D. C. • AUGUST 1969

INVESTIGATION OF THE TURBULENT WIND FIELD BELOW

150M ALTITUDE AT THE EASTERN TEST RANGE

By Alfred K. Blackadar, John A. Dutton,
H. A. Panofsky, and Anton Chaplin

NATIONAL AERONAUTICS AND SPACE ADMINISTRATION

TABLE OF CONTENTS

LIST OF FIGURES

PREFACE

The characteristics of the wind near the ground are of particular significance as a source of aerodynamic loads imposed on vehicles during launch operations. The need for quantitative data and better understanding of the statistical properties of these characteristics has led to the construction of a 150-meter meteorological tower on Merritt Island at the Kennedy Space Center. The present report presents the results of a one-year study of wind data for this site that has been conducted at The Pennsylvania State University.

The principal aim of this study, which is continuing, has been to determine the factors affecting the structure of the wind, wind shear, and associated turbulence so as to permit predictions about the statistical effects of wind on space vehicles, both on the pad and during the first few moments of flight. When the effects of parameters such as wind direction, stability, etc. on the wind shear and turbulence are known, then statistical models of the turbulent environment can be constructed based on the climatology of the relevant parameters.

The research reported here was conducted primarily by H. A. Panofsky, Evan Pugh Professor of Atmospheric Sciences, A. K. Blackadar, Professor of Meteorology, and J. A. Dutton, Associate Professor of Meteorology. Significant contributions were also made by R. T. Duquet, Associate Professor of Meteorology, and by Anton Chaplin, Dennis Deaven, James J. Watts, and Elizabeth Mares, Research Associates in the Department of Meteorology.

The report summarizes nearly all aspects of the research conducted during the first year's study. Not included is a documentation of a computer program "TRANS" that was developed by Duquet (1967) to compute Fourier transforms of series of real numbers and, from the transforms, to provide estimates of spectra and cross-spectra of these series. The program is based on the Cooley-Tukey Fast Fourier Transform algorithm and provides a package of auxiliary subroutines that facilitates the analysis of data. A documentation of this program was issued as a report under the project and is available from the Department.

The data examined in the study consisted of 84 runs, approximately one hour in duration, comprising 0.1 second values of horizontal wind components together with mean wind direction, speed, and temperature at each of six levels on the 150m tower. The tower facility has been discussed in detail by Kaufman and Keene (1968) and will be only briefly summarized below.

a. Terrain features

Figure 0.1 shows the location of the facility with respect to the Saturn V space vehicle launch complex 39. Located about three miles from the Atlantic Ocean, the tower is situated in a well-exposed area free of nearby structures that could interfere with the air flow.

The aerial photograph (Fig. 0.2) of the terrain surrounding the tower (point T) was taken at 1065 meters above mean sea level. In the quadrant from approximately 300 degrees north azimuth with respect to the tower, clockwise around to 90 degrees, the terrain is homogeneous and is covered with vegetation about one-half to one and one-half meters high. Another homogeneous fetch with the same type of vegetation occurs in the 135- to 160-degree quadrant. The areas A (230-300 degrees), B (90-135 degrees), and C (160-180 degrees) are covered with trees from about 10 to 15 meters tall. The fetch from the tower to areas A or C is about 200 meters, and the fetch to area B is about 450 meters. The height of the vegetation over these fetches ranges from one-half to one and one-half meters, as in the area to the north of the tower. To the south-southwest in the 180- to 230-degree quadrant 225 meters from the tower, there is a body of water called Happy Creek.

b. Instrumentation

The complete tower facility comprises two towers, one 18 meters and the other 150 meters high (see Fig. 0.3). The levels on both towers are instrumented with Climet (Model Cl-14) wind sensors. Temperature sensors, Climet (Model -016) aspirated thermocouples, are located at the 3- and 18-meter levels on the small tower and at the 30-, 60-, 120-, and 150-meter levels on the larger tower. Foxboro (Model F-2711AG) dewpoint
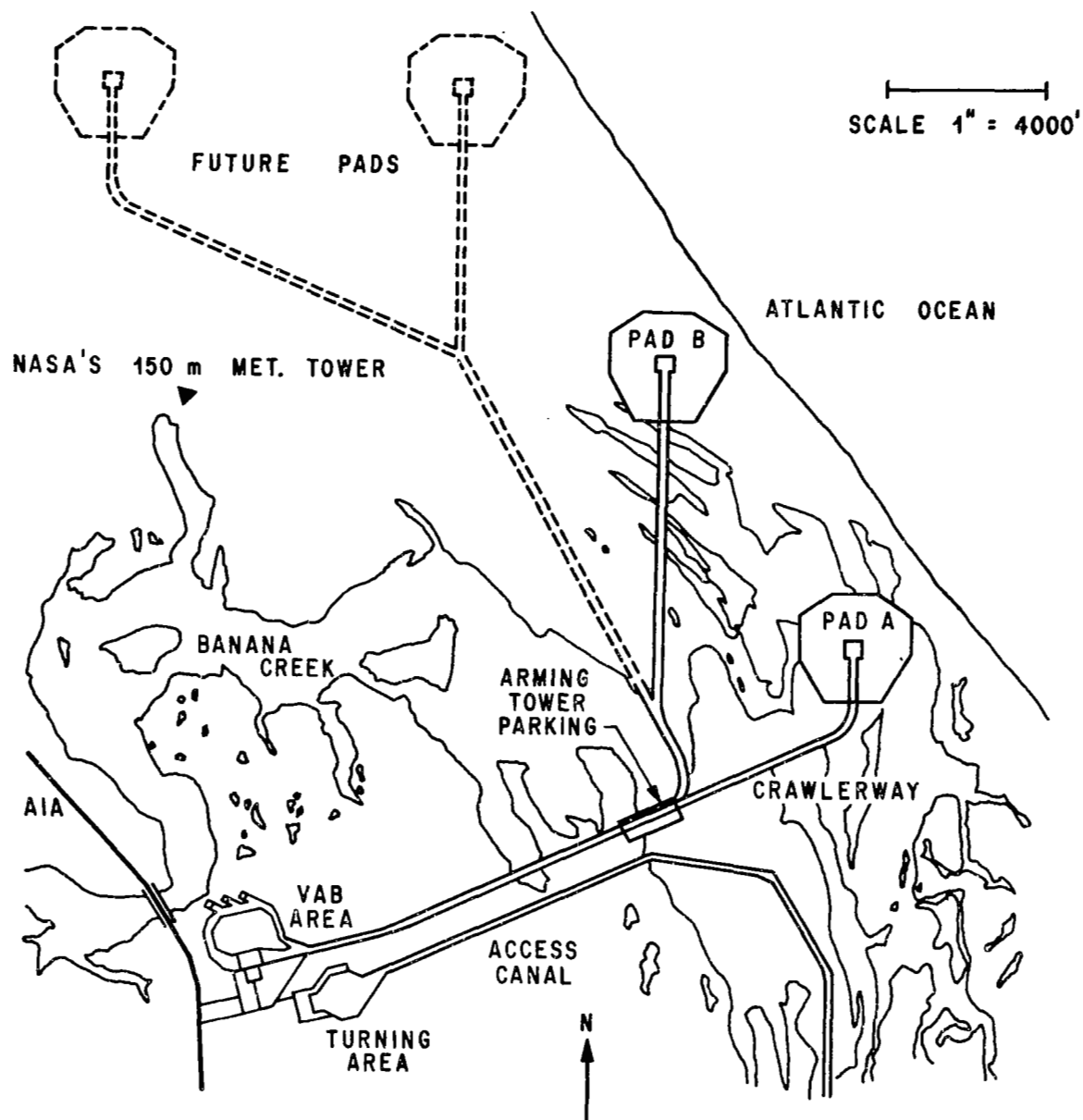
Figure 0.1 Location of the NASA 150-meter tower facility relative to pads A and B in Launch Complex 39 at Kennedy Space Center, Florida.

BOOM HEIGHTS
(meters)

150.0	W ——	—— W, T, T$_d$
120.0	W ——	—— W, T
90.0	W ——	—— W
60.0	W ——	—— W, T, T$_d$
30.0	W ——	—— W, T
18.0	W ——	—— W

N

TOWER →

12' BOOM NE

12' BOOM SW
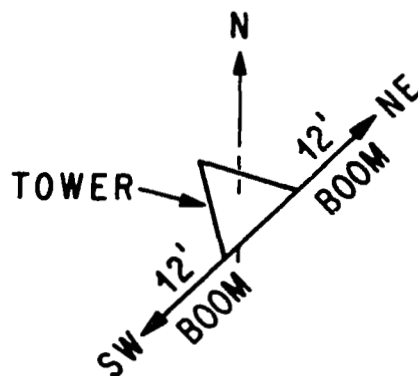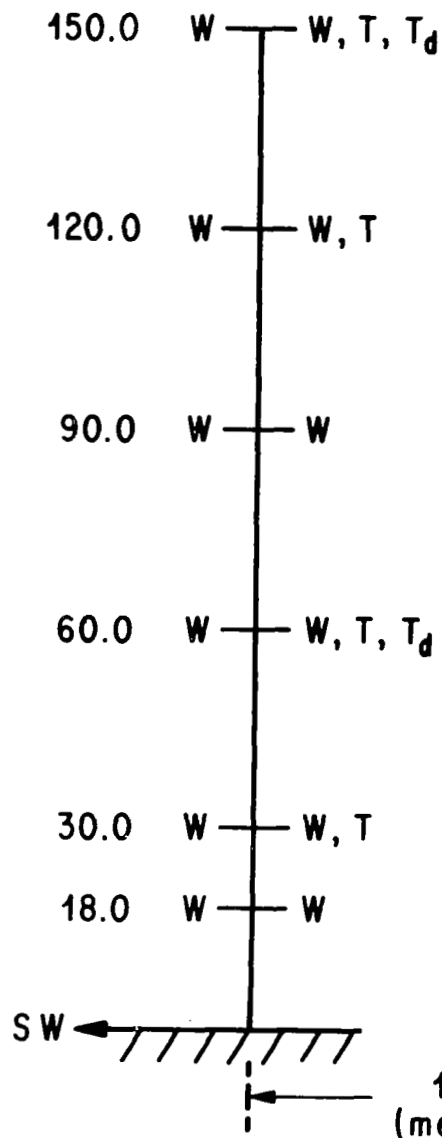
W – WIND SPEED AND DIRECTION
SENSORS
(CLIMET SERIES C1-14)

T – TEMPERATURE SENSOR
(CLIMET ASPIRATED THERMO-
COUPLE SYSTEMS CI-016)

T$_d$ – DEWPOINT TEMPERATURE
SENSOR
(FOXBORO MODEL F-2711AG)

18.0	— W,T
10.0	— W
3.0	— W, T, T$_d$

SW ←——

NE →

|←—— 18.0 ——→|
(meters)
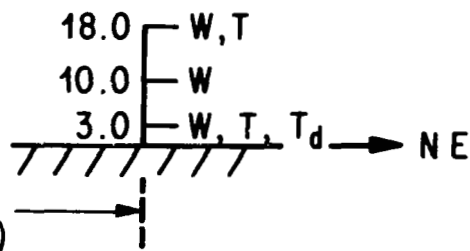
Figure 0.3 Schematic diagram of the NASA tower facility.

x
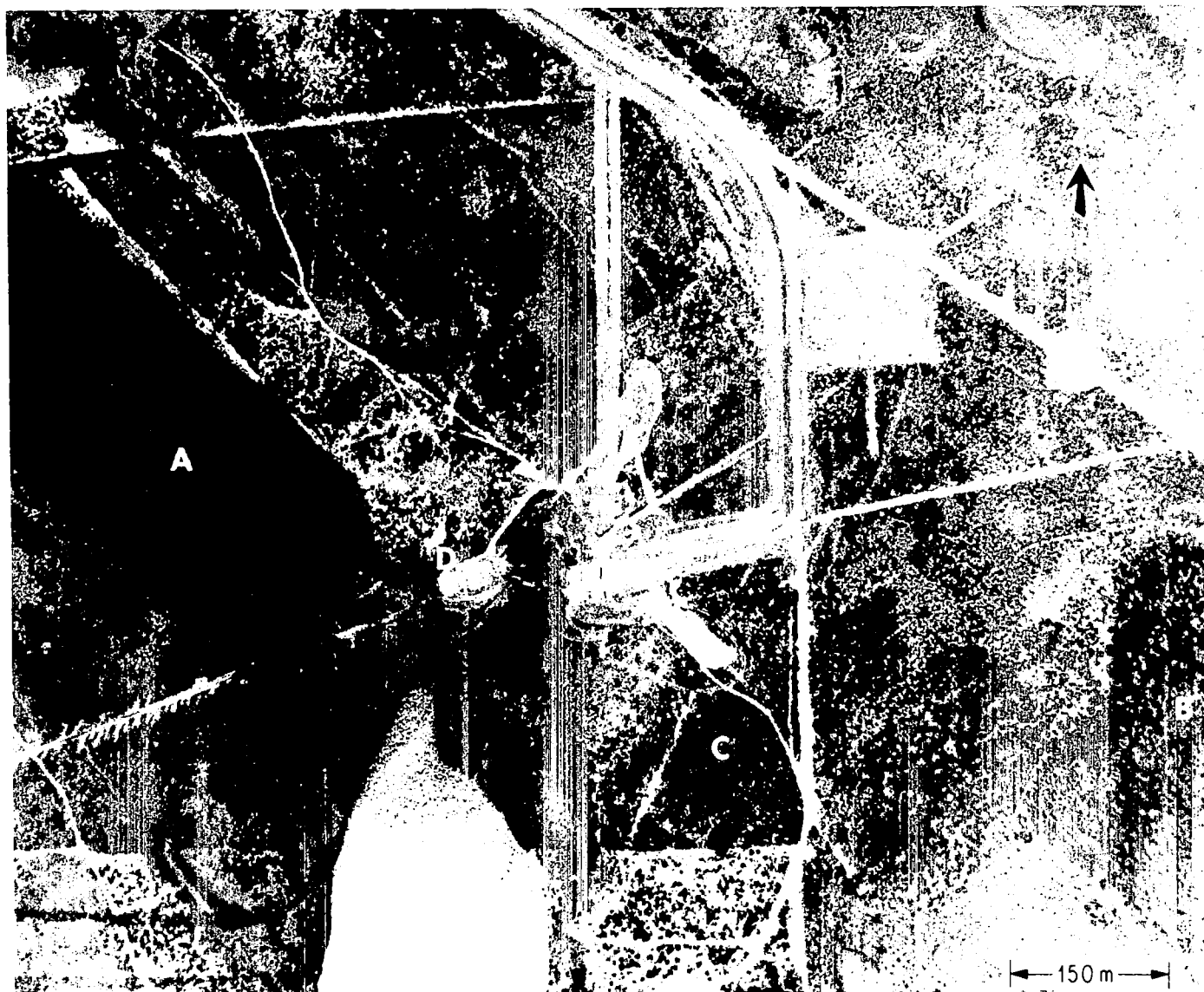
Figure 0.2 Aerial plan of the NASA meteorological tower facility taken at
1065 meters above mean sea level. See text for explanation.

temperature sensors are located at the 60- and 150-meter levels on the large tower and at the 3-meter level on the 18-meter tower. Wind speed and direction data can be recorded on both paper strip charts and analog magnetic tapes with an Ampex FR-1200 fourteen-channel magnetic tape recorder which uses a 14-inch reel. The temperature and dewpoint data are recorded on paper strip charts. To avoid tower interference of the flow, the large tower is instrumented with two banks of wind sensors. The details of how and when one switches from one bank of instrumentation to the other bank were discussed by Kaufman and Keene. During a test in which the wind data are stored on magnetic tape, only one bank of instrumentation is used. This avoids interruption of the wind data signals within any magnetic tape recording period, and thus avoids data-processing difficulties when converting analog tapes to digital tapes.

References

Duquet, R. T., 1967: Documentation of the computer program "TRANS".
    Department of Meteorology, The Pennsylvania State University,
    December, 1967, 24 pp.

Kaufman, J. W., and L. F. Keene, 1968: NASA's 150-meter meteorological
    tower located at the Kennedy Space Center, Florida. NASA Tech.
    Mem. TMX-53699, 22 pp.

NOTE:

I. A PRELIMINARY STUDY OF THE PROBABILISTIC STRUCTURE

OF TURBULENT FORCING OF LAUNCH VEHICLES

John A. Dutton

1.1 Introduction

The loads on the structure and control systems of aerospace vehicles arise from a variety of sources, and the responses to these loads involve interactions by diverse components of the system. Design of a successful vehicle obviously involves determination of the sources of loads and a specification of the characteristics of both the loading and the responses which can be expected.

The interest in this report centers on development of suitable analytical and empirical models of the environment for the study of the forcing of vehicle response by the winds and turbulence which it encounters. The total loading of a vehicle can be separated into two distinct cases. First, there are the responses to the environment which occur while the vehicle is on the launch pad. The second case includes all the loads and responses which occur during the flight of the vehicle.

While the vehicle is on the launch pad, it is subjected to the forces and torques imposed by the ambient wind and turbulence fields. A prototype case is that of a cantilever beam in a turbulent stream. The study of this problem is a relatively straightforward one, particularly because a number of simplifying assumptions may be invoked. We shall refer to the study of vehicle forcing on the launch pad as the static case.

More complex problems are encountered in the attempt to study the loads and responses of a launch vehicle in flight. Two main sources of in-flight loading are inherent in the vehicle and its mission. First, there will be natural oscillatory modes of the structure which may be excited during flight. Second, loads will be imposed by the control system as it attempts to follow an established trajectory. These two sources of loads can themselves lead to catastrophic responses.

A third source of in-flight loads is the environment in which the vehicle must operate. The aerodynamic loadings on the vehicle will be altered when atmospheric turbulence is encountered, and torques induced by shears in both the mean wind and its turbulent component require load-inducing commands from the control system. The environment may provide significant forcing of natural modes in both structural and control components of the vehicle, and due to the possibility that disastrous atmospheric configurations may be encountered, the environment may also be a source of catastrophic response.

On a given launch, both deterministic components of the environment, such as the mean wind profile, and random components, such as the turbulent parts of the motion field, may be important. The aspect which complicates analysis is that the designer must be concerned with the ensemble of possible atmospheric configurations, and thus is forced to view any particular case as a realization of a random process.

Therefore, both the static and in-flight response problems are essentially those of a deterministic system forced by a random environment. The crucial question, in developing adequate design procedures, then, is what information about the atmospheric environments is needed and how can it be used effectively.

1.2 Approaches to the probabilistic study of response

Two approaches, different in spirit but necessarily interrelated, are possible. In the first, the emphasis is placed upon the characteristics of the temporal relationships between the environment and the response. In essence, the response at any time is viewed as a functional depending upon the entire past history of the relevant atmospheric variables. An example of this type of study is the determination of the spectra of responses from the spectra of atmospheric variables. When the characteristics of the functional relating response to the entire past of the forcing are known, it is in principle possible to determine the probabilistic structure of the response, and this permits the designer to assess system reliability on the basis of confidence limits derived empirically from atmospheric data.

The second major approach is to concentrate on the probabilistic structure of the response as determined from the probabilistic characteristics of the forcing, ignoring as much as possible the temporal sequencing of events. For example, a linear system forced by a Gaussian process will itself possess a Gaussian response and thus the statistical characteristics of the response can be determined with the functional relationship between input and output used only to establish relationships between basic statistical parameters such as means and variances; the details of temporal sequencing can be neglected. In this approach the emphasis is on the probabilistic structure of a phase space composed of relevant vehicle and atmospheric variables, and the precise trajectories in the phase space representing actual sequences of events are only of minor interest.

Although this second approach of concentrating on the phase space is the more economical and sophisticated method of contemplating response problems, it is only possible at present in certain simplified situations. The necessity of dealing with nonlinear responses or non-Gaussian forcing in most of the important cases necessitates determination of the structure of these phase spaces by the calculation of numerous trajectories. It is necessary, in effect, to adopt the first approach and to study the temporal sequencing of response as a functional of forcing in sufficient detail that the resulting trajectories are dense enough in the phase space so that its structure can be ascertained.

The first step, regardless of which approach is used, is to determine the statistical structure of the forcing. Thus we first consider the probabilistic characteristics of atmospheric turbulence as revealed by wind measurements at the Kennedy Space Center. Comparisons with some other data on atmospheric turbulence will be made as an aid in establishing the reliability and general applicability of the conclusions.

1.3 Topics to be discussed

Some of the basic theory is reviewed in the next section and the particular difficulties associated with analysis of launch vehicles are considered. The preliminary observational results now available are

4

presented and some conclusions about the probabilistic structure of turbulence justified.

Finally, an approach to the study of the structure of the largest gusts which has particular significance for simulation studies is developed and illustrated with a preliminary sample of data. This approach, which is based on the proper orthogonal decomposition theorem, is then used to establish a theory of the spectra of launch vehicle response.

1.4 Some aspects of response statistics

The most general characterization of the relationship between the response of launch vehicles and the forcing of the atmosphere may be written as

$$(1.1) \qquad \dot{y}_i = Y_i(t; y_1, \ldots, y_n; u_1, \ldots, u_m) \qquad (i = 1, 2, \ldots, n)$$

in which y_i are the response variables, $\dot{y}_i$ their derivatives, u_j are the atmospheric forcing functions, and t is time. Higher order differential systems can always be put in this form by addition of auxiliary variables if necessary. When solutions exist they may be written as functions of time and the initial values $y_i(t_o)$ in the general form

$$(1.2) \qquad y_i(t) = F_i(t; y_1(t_o), \ldots, y_n(t_o))$$

The effect of the forcing variables is now masked in the time dependence indicated. Thus in principle the probabilistic structure of the variables y_i is determined by the statistical characteristics of the forcing variables.

1.5 Consequences of linearity

In many cases, the system (1.1) may be reduced by perturbation theory to a linearized system of equations which may be written as

$$(1.3) \qquad \dot{y} = Ay + Bu$$

where y is now an n x 1 vector of responses, u the m x 1 vector of forcing variables, and A and B the (n x n and n x m) matrices of constant coefficients. Such a system of equations has the _formal_ solution

$$y(t) = e^{At}[\int_{t_o}^{t} e^{-A\tau}Bu(\tau)d\tau + y(t_o)]$$

(1.4)

$$= \int_{t_o}^{t} e^{A(t-\tau)}Bu(\tau)d\tau + y(t_o)e^{At}$$

in which the exponents with matrix arguments may be specifically evaluated with a MacLaurin's series. The usual assumption that $y(-\infty)$ vanishes and the definition of the matrix

(1.5) $$W(t-\tau) = e^{A(t-\tau)}B$$

allows us to write

$$y(t) = \int_{-\infty}^{t} W(t-\tau)u(\tau)d\tau$$

(1.6)

$$= \int_{o}^{\infty} W(\tau)u(t-\tau)d\tau$$

For many aeronautical applications, it can be assumed that (1.6) applies directly to the problem and that due to the lengthy horizontal trajectories of aircraft through turbulence fields assumed to be homogeneous the response y may be treated as a stationary process. The static problem for launch vehicles may also be treated in this manner, although the assumption of stationarity of the forcing is not as well justified. In both cases, emphasis then shifts from (1.6) to the familiar spectral equations, some aspects of which are discussed by Dutton (1968). But for analysis of launch vehicles in flight these assumptions are certainly not valid. For example, it is not realistic to reduce (1.4) to the infinite form (1.6) and furthermore the integral must be calculated along the actual trajectory of

the vehicle through the turbulent field. Thus we must rewrite the basic equation (1.3) as a function of the vehicle trajectory, $\underset{\sim}{x}(t)$, in the form

$$(1.7) \quad \dot{y}(t) = Ay(t) + Bu(\underset{\sim}{x}(t),t)$$

where $u(\underset{\sim}{x},t)$ is the vector of the forcing variables evaluated at position $\underset{\sim}{x}$ and time t. Thus the solution becomes

$$(1.8) \quad y(t) = y(t_o)e^{At} + \int_{t_o}^{t} W(t-\tau)u(\underset{\sim}{x}(\tau),\tau)d\tau$$

If the vector y includes specification of the trajectory, x(t), then (1.8) is not an actual solution to the system (1.7) because the forcing is no longer a function solely of the time but now depends on part of the vector y as well. Thus we have reverted to the form (1.1) and no general method of solution is available.

The appearance of the finite value, t_o, in (1.8) also makes the usual approach to spectral theory, which involves changes in the order of integration, ponderous at best, and points out the difficulties in attempting to develop a form of the usual spectral procedures which would be as useful for launch vehicles as it is for aircraft. Many of these same difficulties, incidentally, appear in the attempt to analyze the statistics of response of V/STOL aircraft.

1.6 Consequences of Gaussian forcing

Let us assume that the control system has sufficient power to achieve an established trajectory without error so that $\underset{\sim}{x}(t)$ is known in advance. (Whether it does or not will, of course, depend upon the wind velocities encountered by the vehicle.) Then $\underset{\sim}{x}(t)$ need not be introduced in the vector y and (1.8) is a solution of the system. Now if the variables $u(\underset{\sim}{x},t)$ were a realization of a Gaussian process, the linear operation in (1.8) would preserve that structure and all of the necessary statistical information about the response could be ascertained from (1.8).

For example, consider the one-variable case and assume that $y(t_o)$ vanishes. Upon assuming that the Gaussian forcing variable has a vanishing expectation at each point (x,t), we find that

(1.9) $\quad E\{y(t)\} = \int_{t_0}^{t} W(t-\tau)\dot{E}\{u(\underset{\sim}{x}(\tau),\tau)\}d\tau = 0$

and that

(1.10) $\quad \dot{E}\{y(t)y(t')\} = \int_{t_0}^{t} W(t-\tau)[\int_{t_0}^{t'} W(t'-\tau')E\{u(\underset{\sim}{x}(\tau),\tau)u(\underset{\sim}{x}(\tau'),\tau')\}d\tau']d\tau$

Thus the probabilistic characteristics of the variable y are those of a Gaussian process with zero mean and variance $\sigma_y^2 = E\{y(t)y(t)\}$ determined with the aid of the weighting function $W(\tau)$ from the correlation function of $u(x,t)$. If $u(x,t)$ is homogeneous in space and stationary in time this correlation becomes

(1.11) $\quad E\{u(\underset{\sim}{x}(\tau),\tau')u(\underset{\sim}{x}(\tau'),\tau')\} = \phi_u(\underset{\sim}{x}(\tau) - \underset{\sim}{x}(\tau'),\tau-\tau')$

but we still cannot conclude that $y(t)$ is stationary to second order because of the presence of the finite limits of integration, t_0, which point out the non-stationary effects to be expected in the initial portions of flight.

For the static case, (1.6) shows that the response is a linear operation on the forcing u. Thus if the forcing is Gaussian, so will the response be Gaussian with mean and variance determined from (1.6) in the manner of (1.9) and (1.10).

Because of the relative simplicity of the analysis of Gaussian processes, the determination of whether turbulence can be so considered is obviously a first requirement.

1.7 Exceedance statistics

Perhaps of more practical importance in design considerations than the basic probability density function of the responses are the exceedance statistics which can be derived from them. The basic concepts of the theory are due to Rice (1939, 1945), and the quantitative interest centers on the frequency with which a given value of the response may be expected to be exceeded.

The development of the theory will be illustrated here by a derivation following Crandall (1963); a thorough and rigorous discussion is given by Cramer and Leadbetter (1967).

Consider a statistical process y(t) defined, for the present, in discrete time at intervals of Δt for a period of length T. We define the quantity N(y) to be the frequency with which the process crosses through the value y with positive slope in unit time. We may write as the probability that a point selected at random will be a point at which y is crossed with positive slope

$$\text{Pr \{crossing of } y\} \quad = \quad \frac{\text{Number of crossings of } y \text{ in T}}{\text{Total number of points in T}}$$

(1.12)
$$= \quad \frac{\text{Number of crossings of } y \text{ in T}}{T/\Delta t}$$

$$= \quad N(y)\Delta t$$

Now let us consider the function y(t), its derivative $\dot{y}(t)$, and a fixed level y_o. If y(t) is sufficiently smooth, then it can cross y_o with positive slope during the time between t and $t + \Delta t$ only if

(1.13) $\quad y(t) \leq y_o$

and

(1.14) $\quad y(t+\Delta t) > y_o$

Upon making Δt small enough, we may use a Taylor's series to rewrite the last condition as

(1.15) $\quad y(t) > y_o - \dot{y}(t)\Delta t$

where $\dot{y}$ must be positive for a crossing with positive slope to occur before $t + \Delta t$.

Thus if $p(y,\dot{y})$ is the temporally invariant joint probability

density function, then we may combine (1.13) and (1.15) to find that

$$
\begin{aligned}
N(y_o)\Delta t \quad &= \quad \mathrm{Pr}\ \{\text{crossing of } y\} \\[4pt]
(1.16) \qquad\qquad &= \quad \int\limits_{o}^{\infty} [\ \int\limits_{y_o - \dot{y}\Delta t}^{y_o} p(y,\dot{y})\,dy\,]\,d\dot{y}
\end{aligned}
$$

To eliminate the dependence on Δt we may differentiate by it to obtain

$$
(1.17) \quad N(y_o) = \int\limits_{o}^{\infty} \dot{y}\,p(y_o - \dot{y}\Delta t, \dot{y})\,d\dot{y}
$$

and then, so that the results apply to continuous time, we let Δt vanish, and for simplicity drop the subscript on y_o. Finally, then, we have the result that

$$
(1.18) \quad N(y) = \int\limits_{o}^{\infty} \dot{y}\,p(y,\dot{y})\,d\dot{y}
$$

Exceedance statistics are generally presented in normalized form

$$
(1.19) \quad N(y)/N(0) = \int\limits_{o}^{\infty} \dot{y}\,p(y,\dot{y})\,d\dot{y} \Big/ \int\limits_{o}^{\infty} \dot{y}\,p(0,\dot{y})\,d\dot{y}
$$

and it is obvious that if the variable y and its derivative are statistically independent so that

$$
(1.20) \quad p(y,\dot{y}) = p_y(y)\,p_{\dot{y}}(\dot{y})
$$

then we have

$$
(1.21) \quad N(y)/N(0) = p(y)/p(0)
$$

Thus for a stationary Gaussian process, in particular, we may employ spectral theory to obtain the correlation

$$(1.22) \quad E\{y\dot{y}\} = \int_{-\infty}^{\infty} i\omega\Phi(\omega)d\omega = 0$$

which vanishes because the spectrum is an even function. Thus (1.20) is valid and we have

$$(1.23) \quad N(y)/N(0) = \exp\left[-\frac{1}{2}(y/\sigma_y)^2\right]$$

in which, from (1.18) we know that

$$(1.24) \quad N(0) = \frac{1}{2\pi}(\sigma_{\dot{y}}/\sigma_y)$$

When the forcing is Gaussian and stationary, then (1.23) will hold for any linear response to that forcing and the variances σ_y^2 and $\sigma_{\dot{y}}^2$ may be calculated from relations of the form (1.6). For more general cases and launch vehicles in particular, the basic concern centers again on the question of how the probabilistic structure of the response is determined from the characteristics of the stochastic forcing functions and the temporal evolution of that probabilistic structure must be taken into account in the theory of exceedance statistics.

1.8 Preliminary results on statistical structure and exceedance statistics of turbulence at Cape Kennedy

Four sets of data measured at six levels at Cape Kennedy were analyzed in detail to obtain information on the probabilistic structure and exceedance statistics of the turbulence fields which affect launch vehicles while they are on the launch pad and in the initial phase of flight.

The original records were wind direction and speed and thus permit definition of a vector wind velocity, $V(t)$. Let $\underset{\sim}{i}$ be a unit vector in the direction of the wind speed, V, over the measurement period, and let $\underset{\sim}{j}$ be a second horizontal unit vector orthogonal and to the left of $\underset{\sim}{i}$.

Longitudinal (u) and lateral (v) components of the turbulent field are thus defined as

(1.25) $\quad u = (\underset{\sim}{V}(t) - \underset{\sim}{V}) \cdot \underset{\sim}{i}$

$\qquad v = \underset{\sim}{V}(t) \cdot \underset{\sim}{j}$

The data used in this section were the original measurements of the component speeds sampled at 10 times per second with linear trends removed. The following quantities were computed from the four sequential records made available:

1. Probability density functions, $p(u)$ and $p(v)$, for the gust velocities as a function of the normalized variates u/σ_u and v/σ_v;

2. Probability distribution functions $P(u)$ and $P(v)$ as a function of the normalized variates, where

(1.26) $\quad P(u) = \int_{-\infty}^{u} p(u')du'$

3. The frequency $N(y)$ of the number of times that levels y were crossed with positive slope per unit time as a function of normalized variates y/σ_y where y/σ_y is either u/σ_u or v/σ_v;

4. The exceedance probability, $N(y)/N(0)$, where $y > 0$;

5. The frequency function for the occurrence of a local maximum or minimum of $y(t)$ in the interval $(y, y + \Delta y)$;

6. The ratio

(1.27) $\quad R = [N(y)/N(0)]/[p(y)/p(0)]$

which is a test of the independence of y and $\dot{y}$.

These quantities, then, reveal whether the velocities have a Gaussian frequency function, what form any departures from a Gaussian law take, and the relevant facts about the exceedance statistics.

The basic data about the four data runs analyzed are given in Table 1.1 and graphs of the listed quantities are displayed in Figs. 1.1 - 1.10. The first two figures, 1.1 and 1.2, are averages.

Figure 1.1 Statistical characterization of the u-component of turbulence at Cape Kennedy
as revealed by the averages of four runs. The plotted numbers represent the
six levels on the tower at which the sensors are mounted, the numbers
increasing with increasing altitude. The abscissas are standardized variables
u/σ_u. The solid line represents the Gaussian case. In the upper right, the
dashed line represents the case of independence between the variable and its
derivative. On the lower right, the ordinate is $\ell n[N(y)/N(0)]$ and the abscissa
is $(u/\sigma_u)^2$.

FREQ DIST

CROSSINGS

$(N(Y)/N(0))/(P(Y)/P(0))$

CUM FREQ DIST

COMB PEAKS PDF

$(Y/SIG(Y)**2$ VS $LOG(NY/N0)$
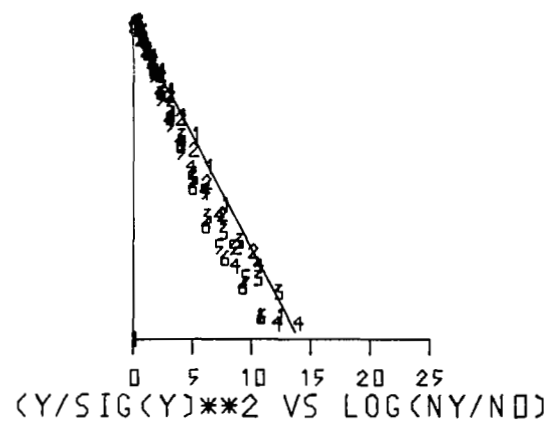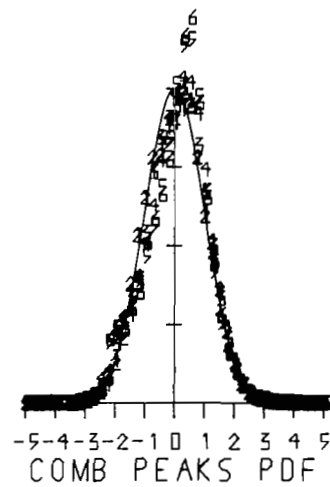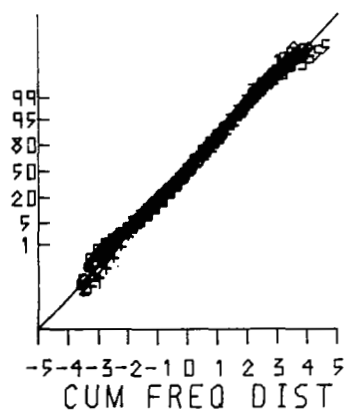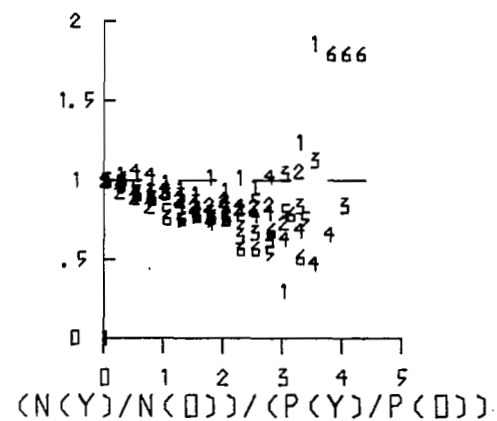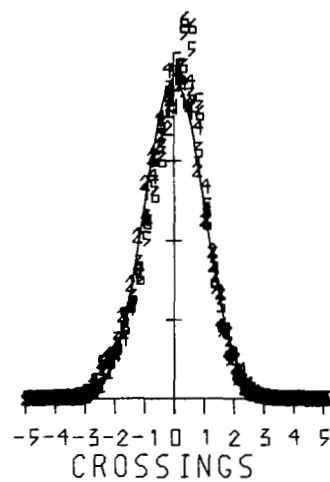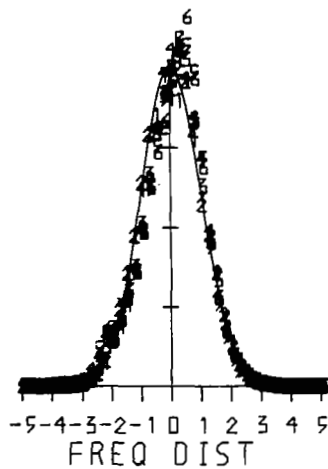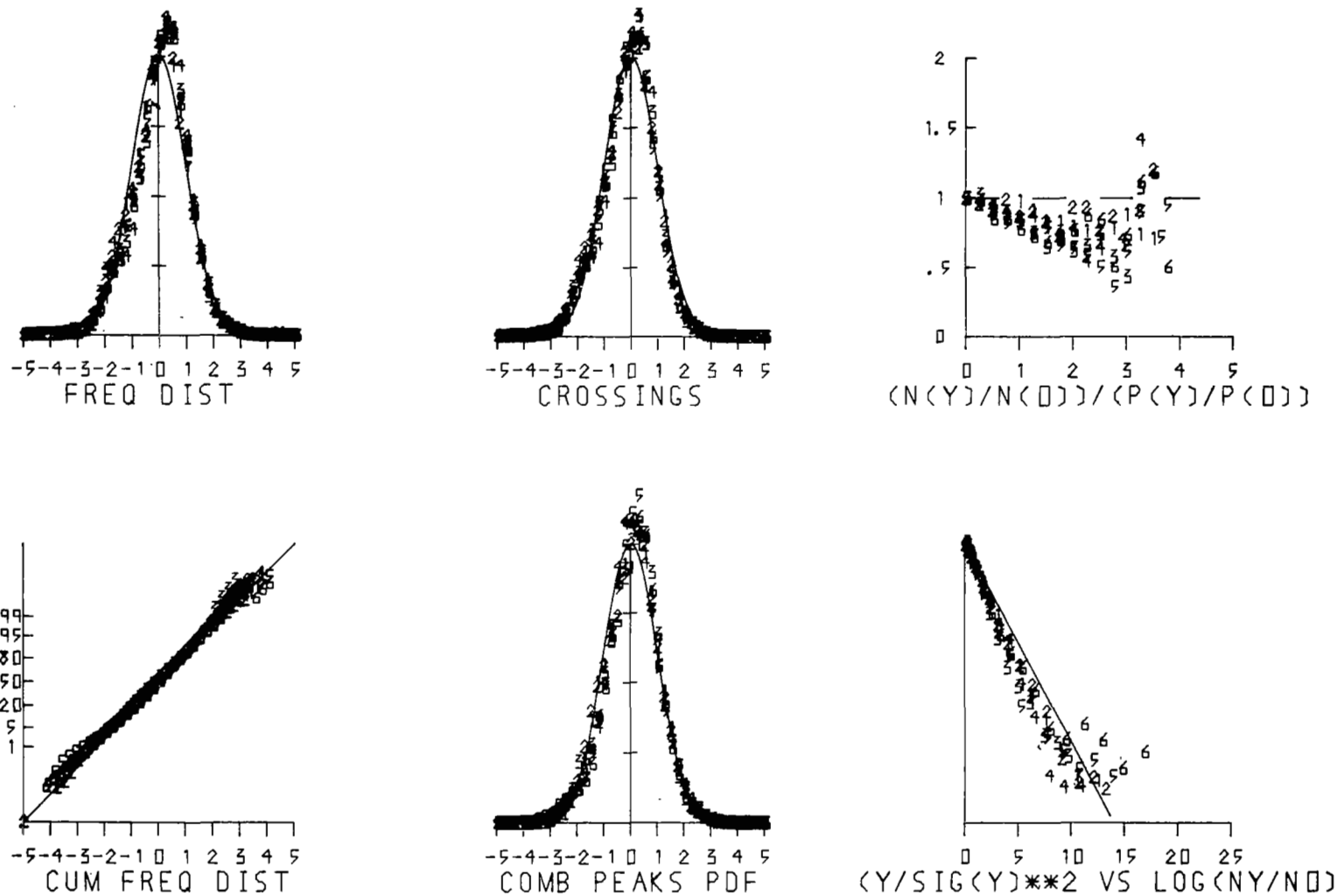
Figure 1.2 Statistical characterization of the v-component of turbulence at Cape Kennedy as revealed by the averages of four runs.
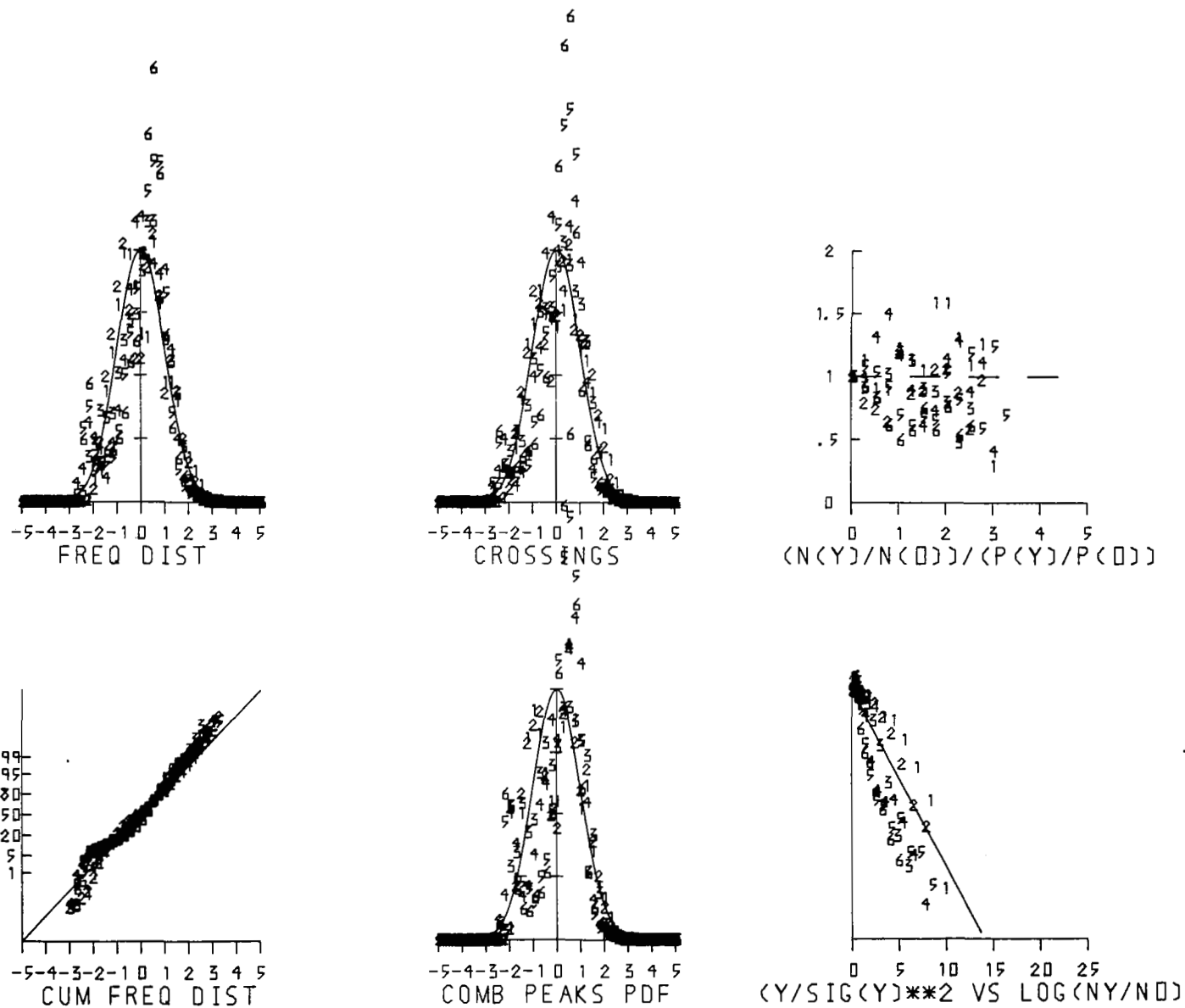
Figure 1.3 Statistics for the u-component of run 029.
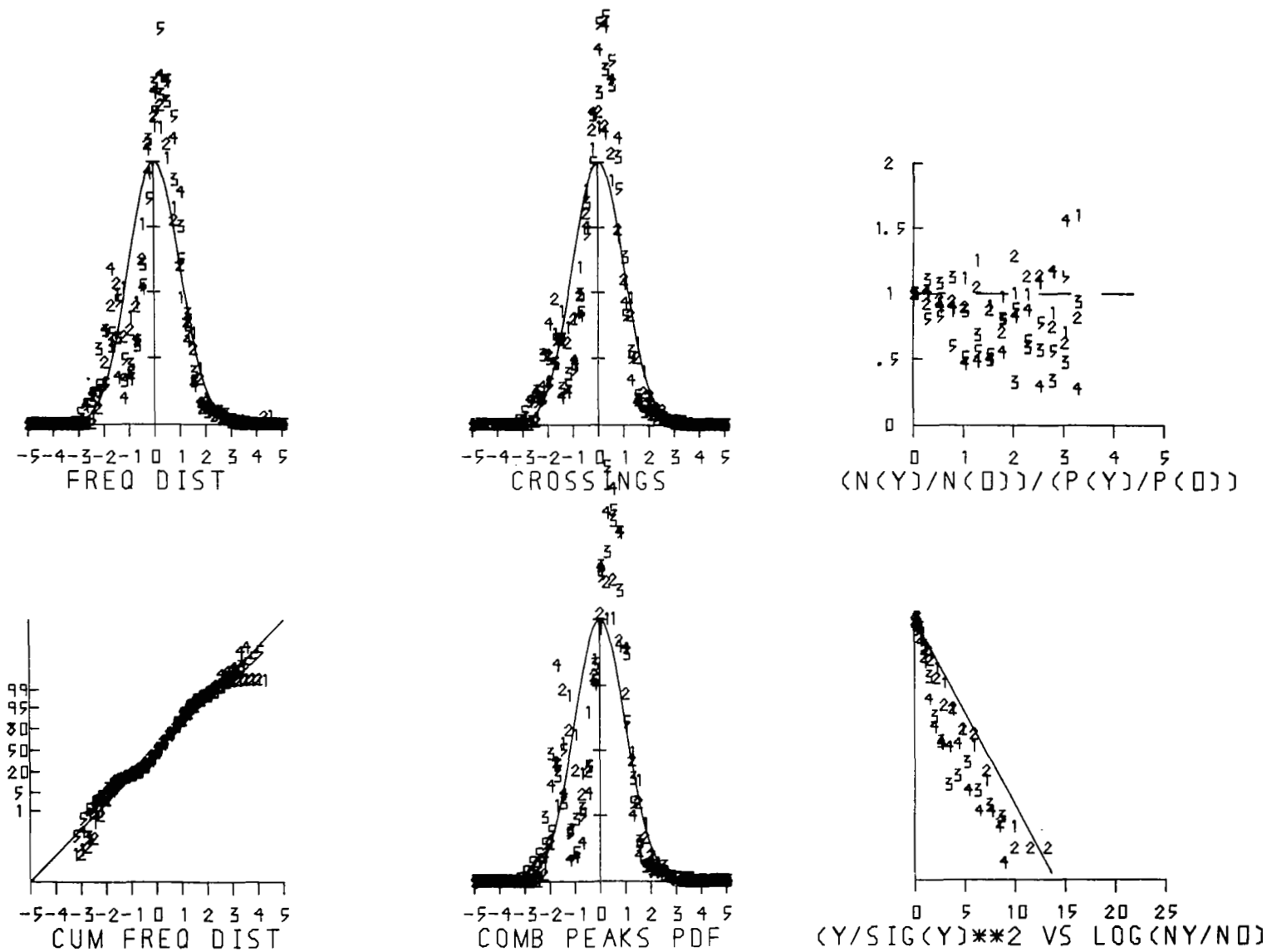
Figure 1.4 Statistics for the v-component of run 029.
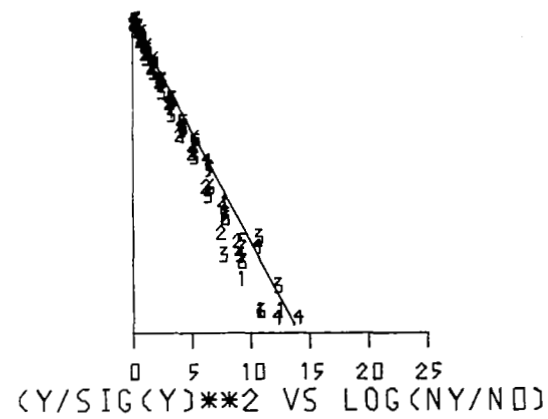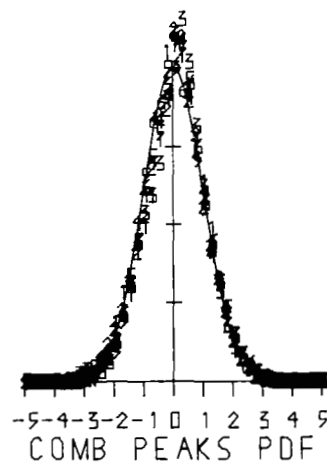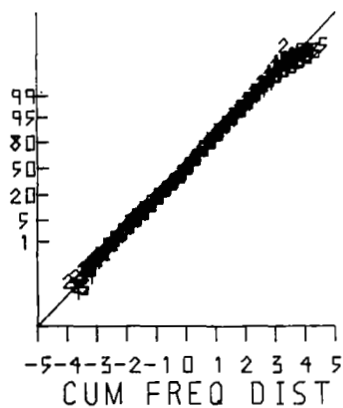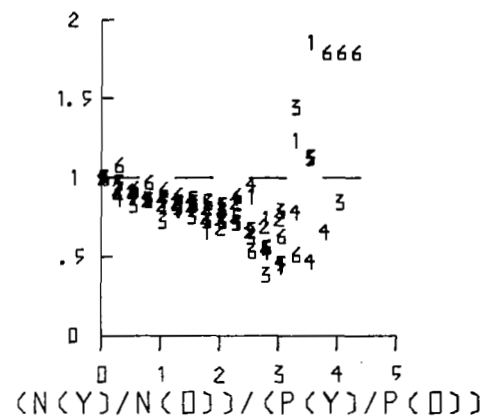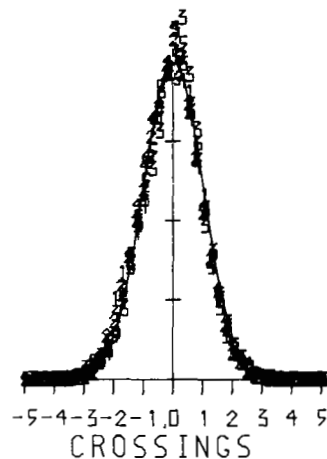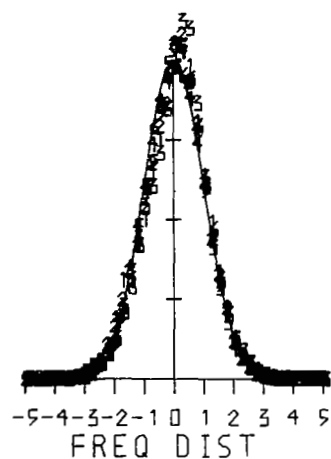
Figure 1.5 Statistics for the u-component of run 067.
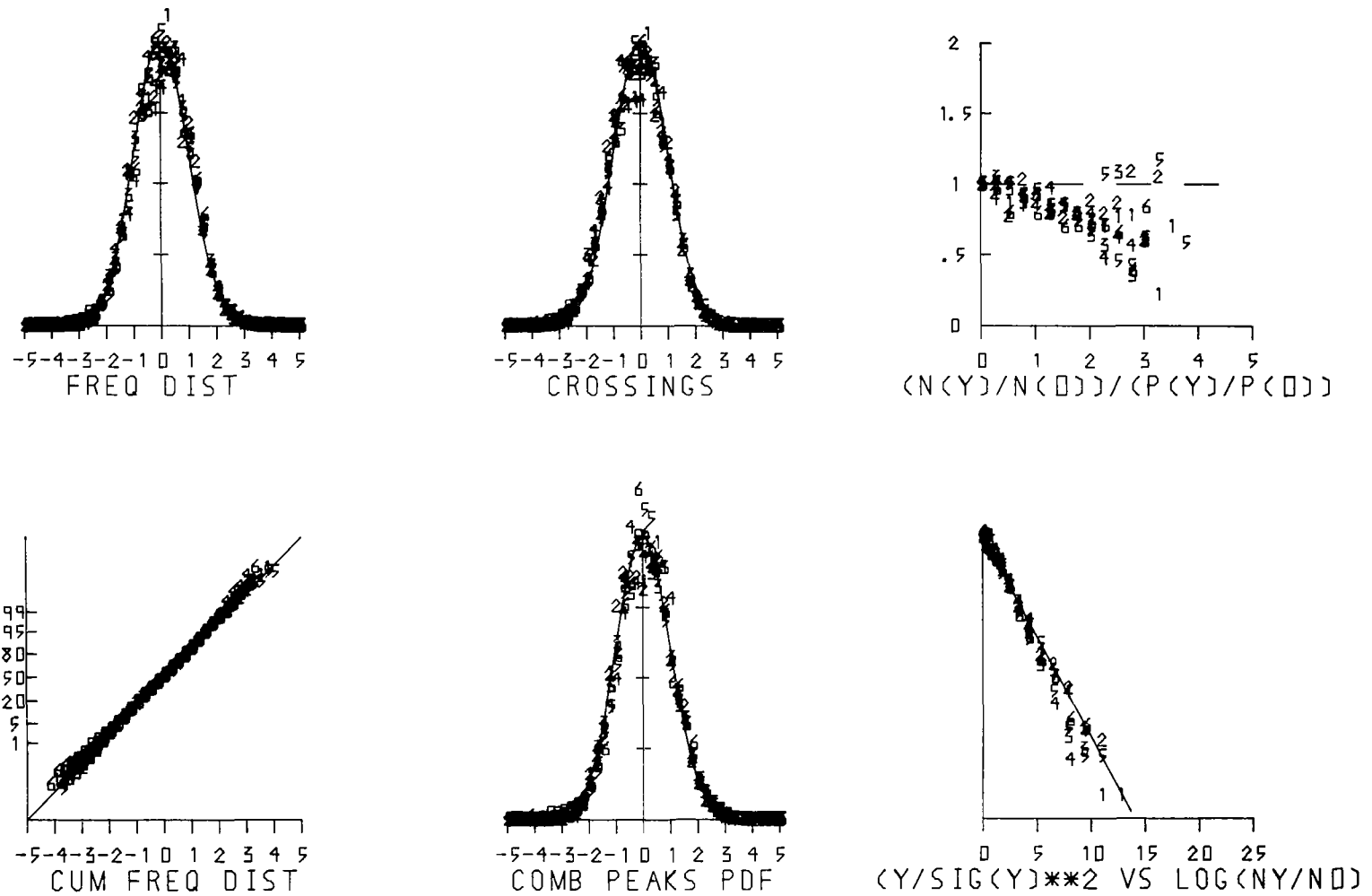
Figure 1.6   Statistics for the v-component of run 067.

Figure 1.7 Statistics for the u-component of run 070.
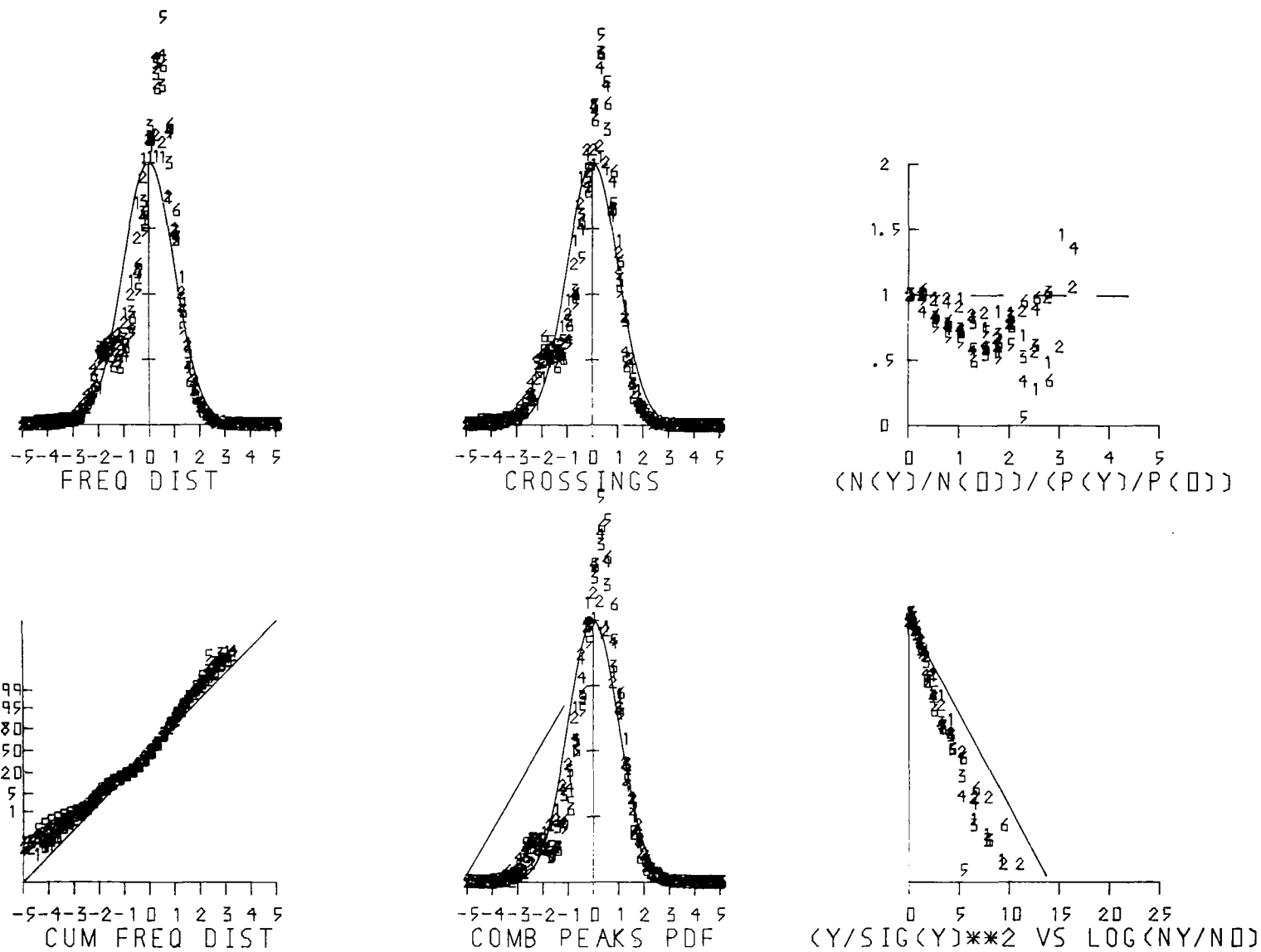
Figure 1.8   Statistics for the v-component of run 070.
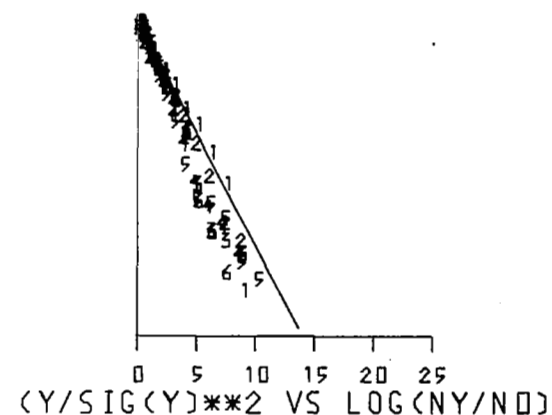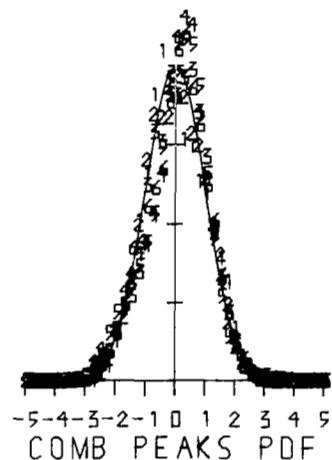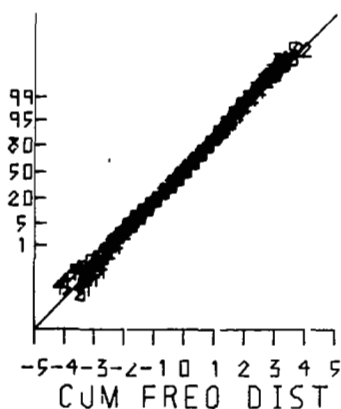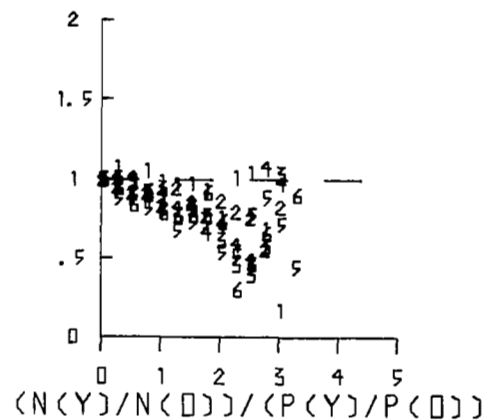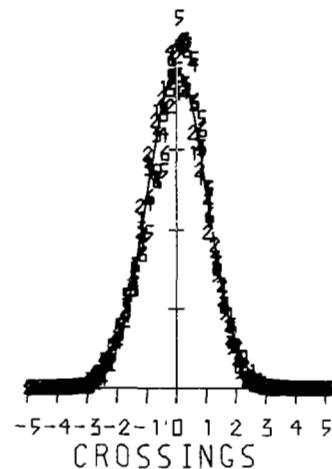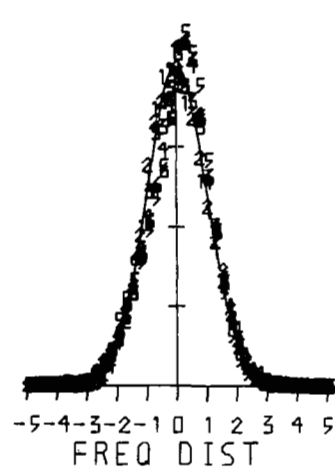
Figure 1.9   Statistics for the u-component of run 075.
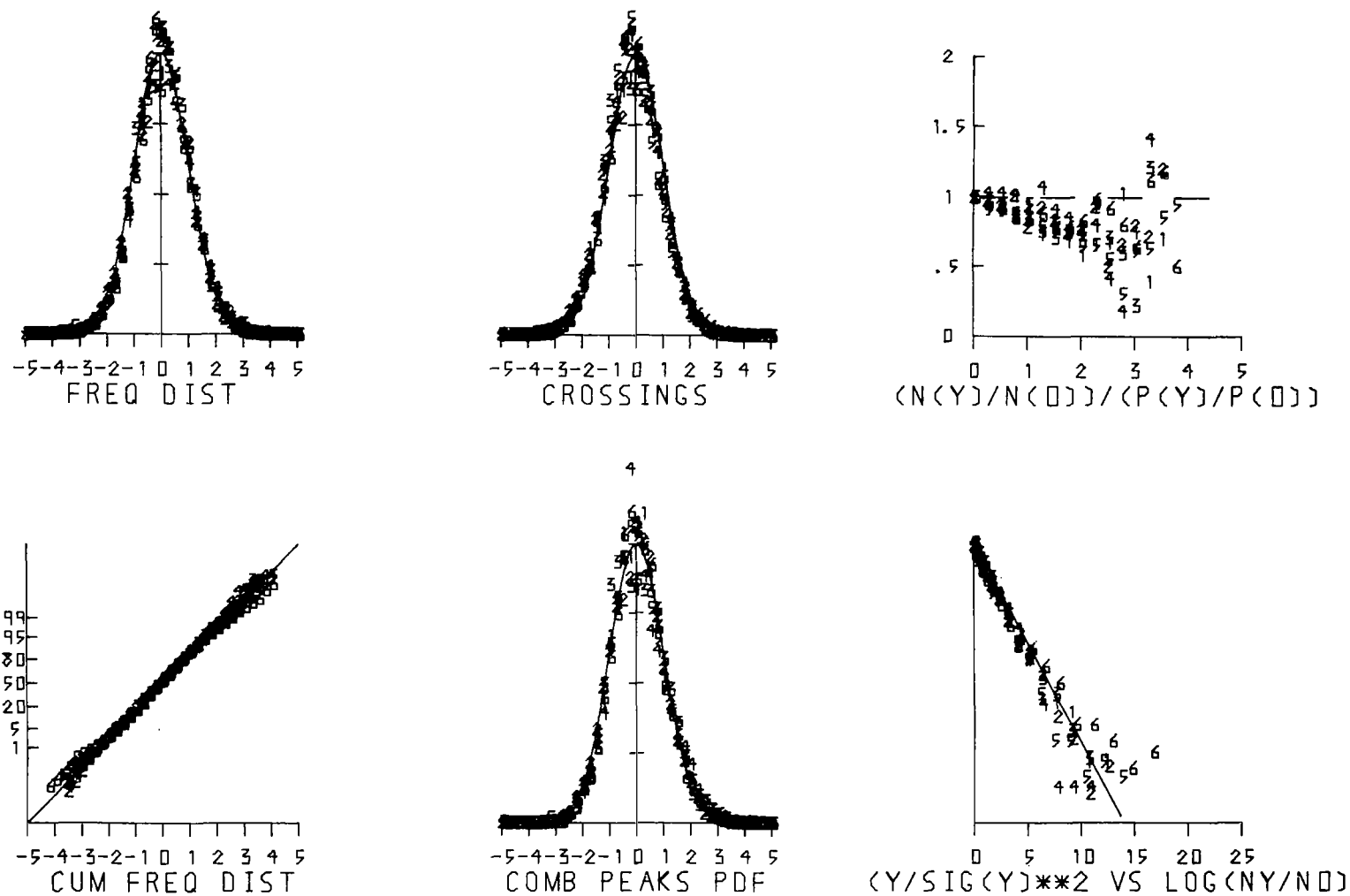
Figure 1.10 Statistics for the v-component of run 075.

Table 1.1 Basic data for the four runs analyzed.

Run	Richardson Number NASA	PSU	18	30	Level (m) 60	90	120	150
					Wind Velocity (m sec^{-1})			
29	-0.19	0.14	3.6	4.2	5.5	6.6	7.2	7.9
67	-0.52	-0.32	7.3	7.7	8.1	8.2	8.3	8.4
70	-0.58	-0.39	6.5	6.9	7.5	7.9	8.0	8.3
75	-0.32	-0.20	5.5	6.1	6.8	7.0	7.2	7.4

computed using the data from the four runs simultaneously. The following conclusions are suggested by this average data:

1. The probability density functions are larger at the origin than a Gaussian function and less than the Gaussian function for y/σ_y in the ranges between 1 to 3 and -1 to -3.

2. The distribution functions show that there is a tendency for a higher probability of large gusts of either sign than in the Gaussian case. The largest departures tend to be at the upper levels.

3. The curve $N(y)$ does not obey the Gaussian law, and $N(y)/N(0)$ tends to fall below the Gaussian curve at first, and then decrease in slope giving a greater probability than for Gaussian cases of crossings of large values.

4. Although strict independence of y and $\dot{y}$ is not verified by the data, it appears that the addition of a function, $C(y)$, to the relation in the form

$$(1.28) \quad \frac{N(y)}{N(0)} = \frac{p(y)}{p(0)} C(y)$$

could be used to make it more accurate than the Gaussian assumption for $N(y)$. This correction would be zero at y equal to zero, and about 2 at

y/σ_y equal to three, and would thus take account of the correlation between y and $\dot{y}$.

The implications of the first three conclusions were discussed in detail by Dutton (1968) where it is shown analytically that a model of turbulence which takes account of its patchy structure appears to be in agreement with the observations. Specifically, it was shown that if the motion fields were composed of patches of fairly intense turbulence with a Gaussian probability density function which were surrounded by regions in which the motions were also Gaussian but with less energy, then the distributions obtained from the entire field would behave qualitatively as enumerated in the first three conclusions.

The wide range of variation possible between individual sets of data is shown in Figs. 1.3 - 1.10. It was perhaps unfortunate that the four samples available had similar mean wind profiles and that three were from definitely unstable conditions. It will be revealing to discover in future analysis whether these statistical characteristics of the turbulence change under neutral and strongly stable conditions, and whether the relationships will change with light and strong mean winds.

1.9 Spectral theory on finite domains and the structure of the largest gusts

The characteristics of the large-scale features of fields of turbulent motion are of considerable interest to both theoreticians and engineers. The analysis of the largest eddies is difficult from a theoretical standpoint because it is unlikely that either homogeneity or isotropy are valid assumptions and no simplifying concepts like that of the universal equilibrium range are available. For the engineer or vehicle designer, the largest gusts are clearly of conern because they contain the majority of the energy and thus have the most pronounced effect on the system.

The mathematical problem to be solved is to find an economical method of representing these largest gusts. There is no *a priori* reason to suppose that any of the classical orthonormal series will be

strikingly efficient in this task, and a tempting objective is to find a set of orthonormal functions which, in some sense, is the most like the functions we are trying to represent. Toward this end, the application of the proper orthogonal decomposition theorem (Loève, 1963) has proven useful in both the study of large-scale meteorological features (for example, Lorenz, 1956; Kutzbach, 1967) and in the study of turbulence (Lumley, 1965). We shall see that it permits a generalization of the notion of spectral decomposition of the variance for functions defined on finite domains, and thus provides a useful method for analysis of launch vehicle response.

1.10   The orthogonal decomposition theorem

To facilitate understanding of the empirical results, we shall develop the relevant theory at some length but make no attempt at bibliographic completeness. Suppose we have an ensemble of functions $\{f\}$ defined on a finite domain ($A \leq x \leq B$) and would like to find one function, ϕ, which is simultaneously the most like all of the functions $\{f\}$ in some sense. The precise nature of ϕ will depend on how we measure resemblance, but if $\{f\}$ were a series of time histories of large gusts with the peak value occurring at the same relative time in the domain of each function f, we could expect ϕ to be a composite "large gust."

A first choice might be to have the correlation between ϕ and f as large as possible upon averaging across the ensemble. This would lead to an attempt to maximize

$$(1.29) \quad r = \int f(x) \phi(x) \, dx$$

in which the definite integral is over the domain of f. However, we are not concerned about signs or magnitudes so that a better choice would be the positive, normalized quantity

$$(1.30) \quad p^2 = \frac{\left| \int f(x) \phi(x) \, dx \right|^2}{\int f^2 \, dx \int \phi^2 \, dx}$$

for which the Schwarz inequality shows that $p^2 \leq 1$.

Finally, to find the best representation of all the functions in {f} simultaneously, we average across the ensemble with the expectation operator to obtain

$$(1.31) \qquad E\{p^2\} = E\left\{\frac{\left|\int f\phi dx\right|^2}{\int f^2 dx \int \phi^2 dx}\right\}$$

Before proceeding to calculate the ϕ which gives a maximum, let us consider another possible measure of resemblance. We might choose

$$(1.32) \qquad D = \int \left|f - \phi\right|^2 dx$$

but this choice leaves open the possibility that, upon averaging over the ensemble, a function ϕ which was like some f and like -f for other functions would be rejected because resemblance to -f would give a large increment to D. Such a function would be useful, however, because its sign could always be changed for any individual f; therefore we want to retain this possibility. Another difficulty with (1.32) is that upon finding a ϕ which extremizes E(D) we would not know whether the extremeum is a maximum or a minimum. This problem has been avoided in (1.31) because the minimum is obviously zero.

To solve the problem, let us observe that $(a - b)^2$ vanishes if a = b and that $(a + b)^2$ does if a = -b so that $(a - b)^2(a + b)^2$ vanishes in either case. Furthermore this quantity must be positive. Upon putting a = λb, we find

$$(1.33) \qquad (a - b)^2(a + b)^2 = 4b^4[(\lambda^2 + 1)^2 - 4\lambda^2]$$

so that, ignoring the magnitude of b, the quantity has extreme values if

$$(1.34) \qquad \lambda(\lambda^2 - 1) = 0$$

Thus it is a maximum for $\lambda = 0$ and a minimum for $\lambda = \pm 1$.

It is convenient to normalize our functions with

$$f_N = f/(\int f^2 dx)^{1/2}$$

(1.35)

$$\phi_N = \phi/(\int \phi^2 dx)^{1/2}$$

and on the basis of the above results we choose

(1.36) $\quad D_N = \int (f_N - \phi_N)^2 dx \int (f_N + \phi_N)^2 dx$

as our measure of similarity. Now it is obvious that with the definition of (1.30)

(1.37) $\quad D_N = 4(1 - p)(1 + p) = 4(1 - p^2)$

so that a maximum of $E(p^2)$ will give a minimum of $E(D_N)$. This makes it clear that the ϕ we hope to find will be more similar than any other function to each f in the ensemble simultaneously -- with similarity to -f considered as beneficial as similarity to f. Similarity, of course, is measured by (1.31) or (1.36).

Therefore, we suppose that a maximizing function exists and we choose some arbitrary function $\delta\phi$ and put

(1.38) $\quad E\{p^2(\epsilon)\} = \overline{p}^2(\epsilon) = E\left\{ \dfrac{\left| \int f(\phi+\epsilon\delta\phi) dx \right|^2}{\int f^2 dx \int (\phi+\epsilon\delta\phi)^2 dx} \right\}$

Because $\overline{p}^2$ is a maximum by definition when $\epsilon = 0$, we expect that

(1.39) $\quad \left. \dfrac{d\overline{p}^2(\epsilon)}{d\epsilon} \right|_{\epsilon=0} = 0$

and so this operation should reveal the nature of the function ϕ. Performing the differentiation and the evaluation at $\epsilon = 0$, we find that

$$(1.40) \quad \int \{ \int E[f(x)f(y)]\phi(x)dx - \overline{p}^2\phi(y) \}\delta\phi(y)dy = 0$$

and because we want ϕ to be the function which gives a maximum, it must be true that (1.40) vanishes for any $\delta\phi$ whatever. This will be true if

$$(1.41) \quad \int E[f(x)f(y)]\phi(x)dx = \overline{p}^2\phi(y)$$

This integral equation, however, rather than specifying one function ϕ generally has a variety of solutions, each associated with a different value of the eigenvalue $\overline{p}^2$. To discover the significance of these solutions, let us name the various values of $\overline{p}^2$ which lead to solutions with λ_n and order them by magnitude with λ_1 being the largest. The solution obtained with each λ_n will be denoted by ϕ_n and we will define the covariance function

$$(1.42) \quad R(x,y) = E\{f(x)f(y)\}$$

Thus the equation becomes

$$(1.43) \quad \int R(x,y)\phi_n(x)dx = \lambda_n\phi_n(y)$$

Now let us take (1.43) and multiply by $\phi_m(y)$ and integrate, which yields

$$(1.44) \quad \int [\int R(x,y)\phi_m(y)dy]\phi_n(x)dx = \lambda_n\int \phi_n(y)\phi_m(y)dy$$

and upon applying (1.43) on the left we obtain

$$(1.45) \quad (\lambda_m - \lambda_n)\int \phi_n(x)\phi_m(x)dx = 0$$

Thus if λ_n and λ_m are distinct eigenvalues, the integral must vanish -- that is to say, the set of functions ϕ_n is orthogonal.

For R(x,y) defined on a finite domain there will be at most a countable number of eigenvalues, and if it should turn out that for some eigenvalue there is more than one associated eigenfunction, the set can always be orthogonalized by the Gram-Schmidt method. Furthemore, all of them may be normalized as in (1.35), so that henceforth we assume that the set of functions ϕ_n is orthonormal.

1.11 Properties of the representation

Now let us use the set of orthonormal eigenfunctions to suppose that any function f in the ensemble can be represented by

$$(1.46) \qquad f(x) = \sum_{k=1}^{\infty} a_k \phi_k(x)$$

Upon multiplication by ϕ_n and integration we find that

$$(1.47) \qquad a_n = \int f(x) \phi_n(x) dx$$

Use of this definition of the coefficient a_n allows us to calculate that

$$(1.48) \qquad E\{a_n a_m\} = E\{\int f(x) \phi_n(x) dx \int f(y) \phi_m(y) dy\}$$

$$= \int [\int R(x,y) \phi_n(x) dx] \phi_m(y) dy$$

$$= \lambda_n \delta_{m,n}$$

Thus the coefficients are uncorrelated across the ensemble, and of equal importance, from (1.46) we find that

$$(1.49) \qquad \int |f(x)|^2 dx = \sum_{j=1}^{\infty} \sum_{k=1}^{\infty} a_j a_k \int \phi_j(x) \phi_k(x) dx$$

$$= \sum_{k=1}^{\infty} a_k^2$$

Upon taking the expectation we find that

(1.50)
$$E\{\int f^2 dx\} = \sum_{n=1}^{\infty} a_n^2 = \sum_{n=1}^{\infty} \lambda_n$$

in which the last equality is verified by reference to (1.48).

Hence we may conclude that the eigenvalues reveal the fraction of the total variance (or mean square), $E\{\int f^2 dx\}$, which is explained by the associated eigenfunction. This permits a more revealing interpretation of the results. We may choose ϕ_1 as the one function most like each of the functions in the ensemble $\{f\}$. But ϕ_1 does not explain all of the variance, so we form a new ensemble of functions $\{f - a_1\phi_1\}$ and find the one function most like these residual functions; the answer will be ϕ_2 and so we consider a new ensemble $\{f - a_1\phi_1 - a_2\phi_2\}$; by induction we thus arrive at our previous results.

To see how well we have represented the totality of functions let us calculate an error, $e_f(N)$,

$$e_f(N) = \int \left| f - \sum_{n=1}^{N} a_n \phi_n \right|^2 dx$$

$$= \int |f|^2 dx - 2 \sum_{n=1}^{N} a_n \int f\phi_n dx + \sum_{n=1}^{N} \sum_{m=1}^{N} a_n a_m \int \phi_n \phi_m dx$$

(1.51)

$$= \int |f|^2 dx - 2 \sum_{n=1}^{\infty} a_n \int f\phi_n dx + \sum_{n=1}^{\infty} a_n^2$$

$$= \int |f|^2 dx - \sum_{n=1}^{\infty} \left| \int f\phi_n dx \right|^2 + \sum_{n=1}^{N} \left| a_n - \int f\phi_n dx \right|^2$$

At this point we have shown that, whatever the nature of the orthonormal series, ϕ_n, the choice (1.47) for a_n will make the error as small as possible. Use of this definition of a_n in the second term of (1.51) then yields

$$(1.52) \qquad e_f(N) = \int |f|^2 dt - \sum_{n=1}^{N} |a_n|^2$$

But now the expectation operator gives as a particular case for the orthonormal eigenfunctions

$$(1.53) \qquad E\{e_f(N)\} = E\{\int |f|^2 dt\} - \sum_{n=1}^{N} \lambda_n$$

Taking account of the relation (1.50) finally allows us to conclude that

$$(1.54) \qquad \lim_{N \to \infty} E\{e_f(N)\} = 0$$

so that in this mean square sense across the ensemble, the series (1.46) gives us a convergent representation of the functions $\{f\}$.

The point is that because the eigenvalues and thus the eigenfunctions can be arranged in order of the fraction of the variance they explain, if the functions in the ensemble $\{f\}$ do have a characteristic structure, the first few eigenfunctions should reveal that structure.

1.12 Optimal character of eigenfunction representations

Before proceeding to the observational results, it will be revealing to look at the question of optimality of the eigenfunction expansion in reverse order. (For a different approach to the final result, see Lorenz, 1956.)

Let us consider an ensemble $\{f\}$ of functions defined on a finite domain and an arbitrary orthonormal sequence of functions, ψ_n. A measure of error in representation with a finite series of the form (1.46) is

$$(1.55) \qquad e_f(N) = \int |f(x) - \sum_{n=1}^{N} \alpha_n \psi_n(x)|^2 dx$$

It is clear from the last equation of (1.51) that whatever the sequence ψ_n, the error will be a minimum if

$$(1.56) \qquad \alpha_n = \int f \psi_n \, dx$$

Therefore, we can consider what happens to the error when we change to functions $\psi_n + \varepsilon \delta \psi_n$ and to coefficients

$$(1.57) \qquad \alpha_n + \varepsilon \delta \alpha_n = \int f(\psi_n + \varepsilon \delta \psi_n) \, dx$$

For the new error, we write

$$(1.58) \quad e_f(N,\varepsilon) = \int \left| f(x) - \sum_{n=1}^{N} (\alpha_n + \varepsilon \delta \alpha_n)(\psi_n + \varepsilon \delta \psi_n) \right|^2 dx$$

and to determine the properties of the set of functions ψ_n which minimizes the error we proceed as before with

$$\left. \frac{d e_f(N,\varepsilon)}{d\varepsilon} \right|_{\varepsilon=0} = 2\int [f(x) - \sum_{m=1}^{N} a_m \psi_m(x)][\sum_{n=1}^{N} (\psi_n(x)\delta\alpha_n + \alpha_n \delta\psi_n(x))] \, dx$$

$$(1.59) \qquad = 2[\sum_{n=1}^{N} \alpha_n \delta\alpha_n - \sum_{m=1}^{N} \sum_{n=1}^{N} \alpha_m \alpha_n \int \psi_m(x)\delta\psi_n(x)\, dx]$$

$$= 2\sum_{n=1}^{N} [\alpha_n \delta\alpha_n - \sum_{m=1}^{N} \alpha_m \alpha_n \int \psi_m(x)\delta\psi_n(x)\, dx]$$

By definition we have

$$(1.60) \quad \alpha_n \delta\alpha_n = \int f(y)\psi_n(y)\, dy \int f(x)\delta\psi_n(x)\, dx$$

so that

$$E[\alpha_n \delta\alpha_n] = E\{\int\int f(x) f(y)\psi_n(y)\delta\psi_n(x)\, dx dy\}$$

$$(1.61) \qquad = \int\int R(x,y)\psi_n(y)\delta\psi_n(x)\, dx dy$$

Thus upon averaging across the ensemble, (1.59) becomes

$$\frac{1}{2} E \left\{ \frac{d\epsilon_f(N,\epsilon)}{d\epsilon} \bigg|_{\epsilon=0} \right\} = \sum_{n=1}^{N} \int_x \{ \int_y R(x,y)\psi_n(y)\,dy$$

(1.62)

$$- \sum_{n=1}^{N} E[\alpha_n \alpha_m]\psi_m(x) \} \delta\psi_n(x)\,dx$$

But the expectation is over {f} so that we interchange the operations and find that it will be true that

(1.63) $$\frac{d}{d\epsilon} E\{e_f(N,\epsilon)\} \bigg|_{\epsilon=0} = 0$$

for any $\delta\psi_n$ whatever provided that for each n we have

(1.64) $$\int R(x,y)\psi_n(y)\,dy - \sum_{m=1}^{N} E\{\alpha_n \alpha_m\}\psi_m(x) = 0$$

A particular solution to this set of equations is

(1.65) $$\int R(x,y)\psi_n(y)\,dy = E\{\alpha_n^2\}\psi_n(x)$$

because upon using this relation, (1.64) may be written as

(1.66) $$E\{\alpha_n^2\}\psi_n(x) = \sum_{m=1}^{N} E\{\alpha_m \alpha_n\}\psi_m(x)$$

and upon multiplication by ψ_k and integration we find that

(1.67) $$E\{\alpha_n^2\}\delta_{nk} = \sum_{m=1}^{N} E\{\alpha_m \alpha_n\}\delta_{mk} = E\{\alpha_k \alpha_n\}$$

Thus, if the functions ψ_n are the eigenvectors of (1.65) then (1.67) is true, and upon use of this relation, (1.64) becomes precisely the equation, (1.65), which determined the functions ψ_n.

The interpretation of this result is that the mean square error, (1.55), averaged across the ensemble will be a minimum for any fixed number of terms, N, provided we use the eigenfunctions of (1.65) as the orthonormal set. The Eq. (1.65) is, obviously, identical to the eigenvalue problem, (1.41), and so the functions ψ_n which give the best representation in this sense are identical to the functions ϕ_n.

1.13 Variance spectra

It is of considerable importance to note that values of a_n^2 or $E(a_n^2)$ give a spectral representation which shows how the variance of an individual function or of the ensemble is distributed over the set of eigenfunctions. To pursue this further, let us return to (1.43) and expand the domain of definition to $(-\infty, \infty)$. Now it is possible to add a further condition that the ensemble be second order stationary so that

$$(1.68) \qquad R(x,y) = R(x-y)$$

and thus (1.43) becomes (provisionally)

$$(1.69) \qquad \int_{-\infty}^{\infty} R(x-y)\phi_n(x)\,dx = \lambda_n \phi_n(y)$$

But this integral equation on an infinite domain need not have a countable number of discrete eigenvalues; they may in fact become continuous. Let us therefore replace n with a continuous variable, ω, and rewrite the equation in the form

$$(1.70) \qquad \int_{-\infty}^{\infty} R(x-y)\phi(\omega,x)\,dx = \lambda(\omega)\phi(\omega,y)$$

We see now that the choice

$$(1.71) \qquad \phi(\omega,x) = e^{-i\omega x}$$

leads to

$$(1.72) \qquad \int_{-\infty}^{\infty} R(x-y)e^{-i\omega(x-y)} dx = \int_{-\infty}^{\infty} R(\tau)e^{-i\omega\tau} d\tau = \lambda(\omega)$$

Thus $\lambda(\omega)$ is the Fourier transform of the correlation function, and except for a constant factor, the function $\lambda(\omega)$ is the usual power spectrum for a stationary process.

The proper orthogonal decomposition theorem, then, gives us a means of defining a spectrum which is appropriate to an ensemble of functions defined on a finite domain. The spectrum thus obtained becomes the classical one when the theory is expanded to stationary functions on an infinite domain. We shall show presently that this spectrum for ensembles defined on finite domains can be of considerable importance in the study of launch vehicle response.

1.14 Representation of the largest gusts

The methods developed in this section were applied to one of the four runs analyzed in Section 1.8 to determine if the largest gusts at Cape Kennedy had a characteristic structure.

The data at each level for Run 067 were examined by computer to find the 10 largest gusts for each component at each level. This operation yielded 60 large gusts for each component, and data for a 3,000-ft sample were extracted from the entire record with the peak value at the center. Letting n represent the nth such sample, the correlation matrix

$$(1.73) \qquad R(x_i, x_j) = \frac{1}{N} \sum_{n=1}^{N} u_n(x_i) u_n(x_j)$$

was then computed. This correlation matrix was used in a summation form of (1.43) along with a standard matrix eigenvalue routine to determine the eigenvalues, λ_n, and the eigenvector, $\{\phi_n\}$.

The first eigenfunctions for both the u and v components are shown in Fig. 1.11. These eight eigenfunctions explain at least 97 percent

EIGENFUNCTIONS FOR PEAKS, NASA U-COMP

EIGENFUNCTIONS FOR PEAKS, NASA V-COMP
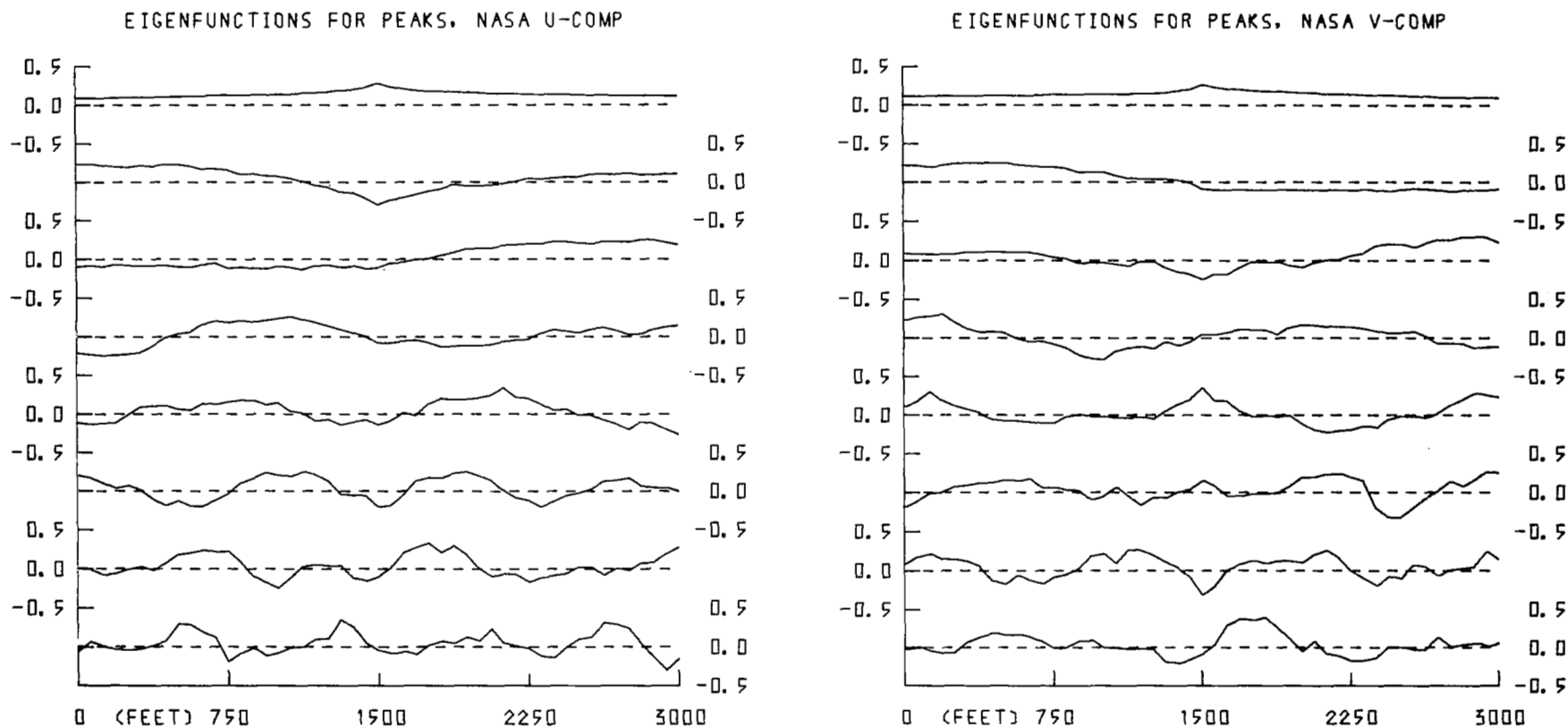
Figure 1.11   Empirical orthogonal functions representing the 10 largest gusts at each of six
levels for run 067.   The functions are arranged with the amount of variance
explained decreasing from top to bottom.

of the variance in each component. The spectral estimates, or eigen-values, are shown in Table 1.2.

A comparison of the largest gusts themselves and the representa-tions obtained with these first eight eigenfunctions is shown in Fig. 1.12.

It is of considerable interest to compare both these eigenfunctions and the large gusts themselves to those found in data measured with aircraft at higher altitude and discussed by Dutton, Deaven and Thompson (1969), and Dutton (1968). The first few longitudinal eigen-functions and the first eigenfunction for the lateral component for these data are similar to those found in clear-air turbulence, but the second eigenfunction for the lateral components of the Cape Kennedy turbulence data is a departure from both the Cape Kennedy longitudinal case and the aircraft case. The most logical place to seach for an explanation of the variation is in the differing effects of buoyancy on the clear-air turbulence and the Cape Kennedy wind field.

The large gusts from the aircraft data appeared to fall into two classes. In the first, the peak was relatively isolated and to some degree one of several large peaks in a quite irregular record. In the second class, the largest peak was the culmination of a fairly slow and regular rise to a maximum which was not markedly above the surrounding values. The large gusts isolated here are in the second class. This may be due to the possibility that the first class arises in aircraft data by records being obtained on runs which pass through the boundaries of a turbulent zone, thus giving rise to alternating samples of turbulent and non-turbulent motion.

It is pointed out by Dutton (1968) that the use of these eigen-functions should provide an economical means of representing the critical characteristics of turbulence for use an inputs to simulation studies. Further work on this possibility is now being planned.

1.15 Spectra of launch vehicle response

The classical theory of variance spectra does not apply to launch vehicle responses in flight because it cannot be assumed, and generally is not true, that the covariance function

Table 1.2 Eigenvalues for large gusts (Run 067).

	Order of Eigenvalue (n)											
	1	2	3	4	5	6	7	8	9	10	11	12
u-component												
$\lambda_n = E\{a_n^2\}$	125.0	6.7	4.8	2.04	1.15	1.05	0.68	0.57	0.48	0.43	0.33	0.29
$\sum_{k=1}^{n} \lambda_k$	125.0	131.7	136.5	138.6	139.7	140.7	141.4	142.0	142.5	142.9	143.3	143.8
$\sum_{k=1}^{N} \lambda_k$	146											
v-component												
λ_n	73.3	6.2	2.5	1.1	0.71	0.58	0.50	0.43	0.31	0.27	0.23	0.18
$\sum_{k=1}^{n} \lambda_k$	73.3	79.6	82.1	83.2	83.9	84.5	84.9	85.3	85.6	85.9	86.1	86.3
$\sum_{k=1}^{N} \lambda_k$	87.8											
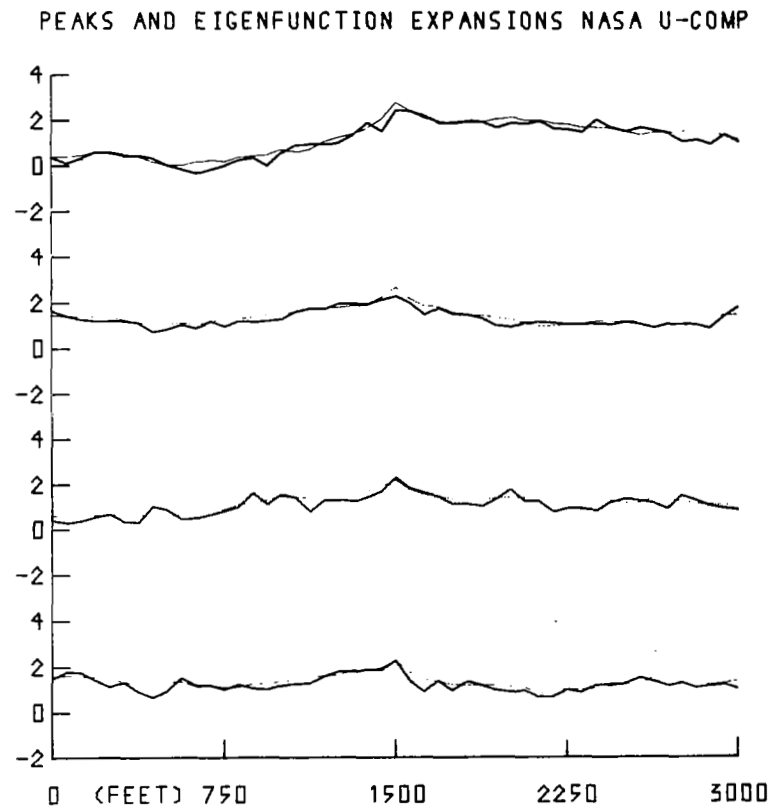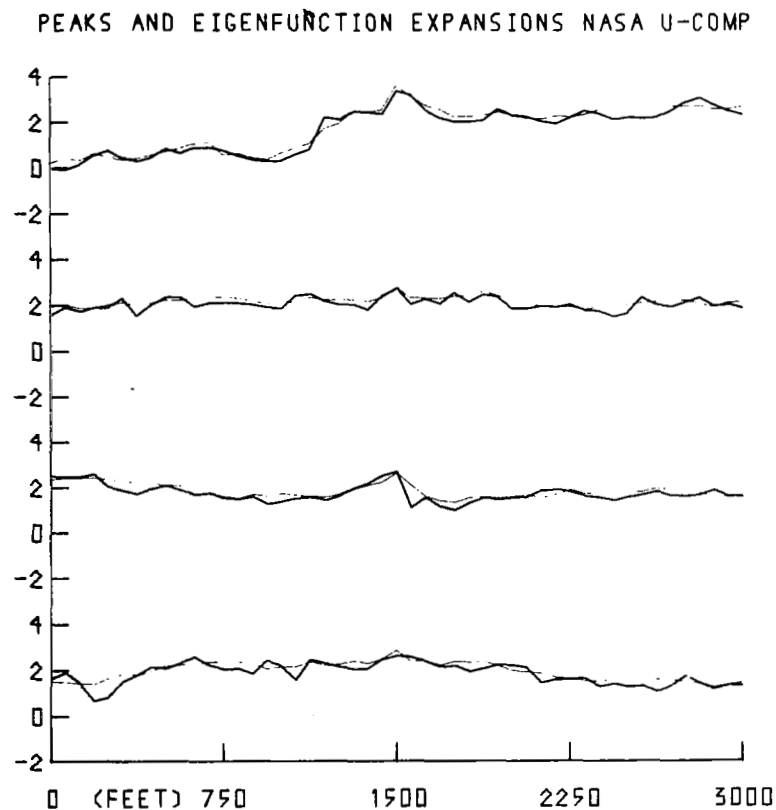
Figure 1.12 Expansions of the four largest gusts in the u- and v-components of run 067 with the empirical orthogonal functions. The heavy solid line is the original data, the light line the expansion utilizing the first eight empirical functions.

(1.74) $\quad R_y(t,t') = E\{y(t)y(t')\}$

is stationary, as was pointed out following (1.10). The basic problem, naturally, is that the responses are defined on a finite domain, but because the proper orthogonal decomposition theorem applies to such a situation it permits us to develop a spectral theory for vehicle responses.

According to (1.10) we have

(1.75) $\quad R_y(t,t') = \int_{t_o}^{t} \int_{t_o}^{t'} W(t-\tau)W(t-\tau') \, R_u(\underset{\sim}{x}(\tau),\tau;\underset{\sim}{x}(\tau'),\tau')d\tau d\tau'$

in which

(1.76) $\quad R_u(\underset{\sim}{x}(\tau),\tau;x(\tau'),\tau') = E\{u(x(\tau),\tau)u(\underset{\sim}{x}(\tau'),\tau')\}$

Thus, the orthonormal eigenfunction representation of the class of responses $y(t)$ can be determined over the domain (t_o,T) from

(1.77) $\quad \int_{t_o}^{T} R_y(t,t')\psi_n(t')dt' = \gamma_n\psi_n(t)$

and we shall have, as before,

(1.78) $\quad y(t) = \sum_n b_n\psi_n(t)$

with

(1.79) $\quad E\{\int y^2(t)dt\} = \sum_n E\{b_n^2\} = \sum_n \gamma_n$

Thus, (1.79) gives a spectrum for the ensemble of responses which, according to (1.75) depends ultimately upon the characterization of the response by the weighting function, $W(\tau)$, and upon the

characteristics of the turbulent motion as specified by the covariance matrix along the trajectory. Hence the problem is to determine a covariance matrix for turbulent motion such that the important features of the turbulent fields are characterized adequately. The theory of proper orthogonal decomposition applies in any number of dimensions, so that if we could determine the space-time covariance function

$$(1.80) \qquad R(\underset{\sim}{x},t;\underset{\sim}{x}',t') = E\{u(\underset{\sim}{x},t)u(\underset{\sim}{x}',t')\}$$

we would have the general eigenvalue problem or the finite domain $(\underset{\sim}{X},T)$

$$(1.81) \qquad \underset{X}{\iiint} \int_{t_o}^{T} R_u(\underset{\sim}{x},t;\underset{\sim}{x}',t')\phi_n(\underset{\sim}{x}',t')dx'dy'dz'dt' = \lambda_n\phi_n(\underset{\sim}{x},t)$$

The solutions to this equation would give the expansion

$$(1.82) \qquad u(\underset{\sim}{x},t) = \sum_n a_n\phi_n(\underset{\sim}{x},t)$$

and with this we would obtain the representation of the covariance matrix in the form

$$(1.83) \qquad R_u(\underset{\sim}{x},t;\underset{\sim}{x}',t') = \sum_n \lambda_n\phi_n(\underset{\sim}{x},t)\phi_n(\underset{\sim}{x}',t')$$

It may be pointed out here that certainly some problems in launch vehicle response will require simultaneous consideration of the effects of various components of the turbulence field. The above representation will then have to be expanded to include the covariance function $R_{ij}(\underset{\sim}{x},t;\underset{\sim}{x}',t') = E\{u_i(\underset{\sim}{x},t)u_j(\underset{\sim}{x}',t')\}$ for the ith and j^{th} components. The results (1.81) through (1.83) will become valid for this case if given an appropriate formulation in tensor or matrix notation; for details, see Lumley (1965).

The relation equivalent to (1.83) for the response is clearly

(1.84) $R_y(t,t') = \sum_k \gamma_k \psi_k(t) \psi_k(t')$

and the spectral estimate γ_n is obtained by integration

(1.85) $\gamma_n = \int_{t_o}^{T} \int_{t_o}^{T} R_y(t,t') \psi_n(t) \psi_n(t') dt dt'$

in accord with (1.77).

The eigenfunctions, $\phi(\underset{\sim}{x},t)$, which represent the four-dimensional turbulent field, also serve to specify the covariance matrix along the vehicle trajectory, $\underset{\sim}{x}(t)$, so that (1.75) may now be written with the aid of (1.83) as

(1.86) $R_y(t,t') = \sum_k \lambda_k \int_{t_o}^{t} \int_{t_o}^{t'} W(t-\tau) W(t'-\tau') \phi_k(\underset{\sim}{x}(\tau),\tau) \phi_u(\underset{\sim}{x}(\tau'),\tau') d\tau d\tau'$

Therefore, the spectral estimate, γ_n, of the fraction of variance associated with the nth eigenfunction becomes

(1.87) $\gamma_n = \sum_k \lambda_k \{ \int_{t_o}^{T} \psi_n(t) [\int_{t_o}^{t} W(t-\tau) \phi_k(\underset{\sim}{x}(\tau),\tau) d\tau] dt \}$

$\cdot \{ \int_{t_o}^{T} \psi_n(t') [\int_{t_o}^{t} W(t'-\tau') \phi_k(\underset{\sim}{x}(\tau'),\tau') d\tau'] dt' \}$

Upon reversing the order of integration, we define

(1.88) $I_{n,k} = \int_{t_o}^{T} [\int_{t}^{T} \psi_n(t) W(t-\tau) dt] \phi_k(\underset{\sim}{x}(\tau),\tau) d\tau$

and hence obtain from (1.87) the relation

(1.89) $\gamma_n = \sum_k \lambda_k (I_{n,k})^2$

The values of $(I_{n,k})^2$ show how the energy represented by λ_k and its associated eigenfunction are transferred to γ_n and its eigenfunction.

Neglecting questions of computational feasibility, we have thus shown that if $R_u(x,\tau; x',\tau')$ is known and summarizes the covariance characteristics of turbulent fields to be encountered by launch vehicles, then upon being given weighting functions for the responses of interest, it is possible to obtain an estimate of the distribution of variance which serves to replace the classical power spectrum, which unfortunately, is not applicable to this case.

In order to obtain some simplification of the procedure, let us assume that the first N terms of the expansion (1.83) will suffice and let us put

$$(1.90) \qquad J_k(t) = \int_{t_o}^{t} W(t-\tau)\phi_k(x(\tau),\tau)d\tau$$

Then from (1.86) we obtain the finite representation

$$(1.91) \qquad R(t,t') = \sum_{k=1}^{N} \lambda_k J_k(t) J_k(t')$$

Now our integral Eq. (1.77) has a kernel of finite rank and may be written as

$$(1.92) \qquad \int_{t_o}^{T} [\sum_{k=1}^{N} \lambda_k J_k(t) J_k(t')]\psi_n(t')dt' = \gamma_n \psi_n(t)$$

$$n=1,\ldots N$$

The eigenvalues and eigenvectors for the responses are found from (1.92) with the approximate kernel, $R(t,t')$, given by (1.91).

Thus from knowledge of the eigenvalues and eigenfunctions for the turbulent field and the weighting function we are able to obtain explicit values for γ_n and also determine the associated eigenfunctions. This gives a spectral characterization of the response to turbulence. Moreover, once the γ_n and ψ_n are determined from (1.92) we can use (1.88) to find $I_{n,k}$ and thus can study how energy is transferred to the response.

1.16 Toward development of adequate response statistics

In the introduction it was pointed out that two approaches to the development of predictions of the probabilistic structure of launch vehicle responses are possible. In the first, the emphasis is on the temporal sequencing of events; in the second, primary attention is devoted to study of probabilistic relations in a suitable phase space.

The fact illustrated in Section 1.8 that the turbulent velocities cannot be considered a realization of a Gaussian process would seem to preclude the second approach at the present time. The development of a theory of in-flight launch vehicle response spectra which makes available a methodology for attempting the first approach was given in Section 1.9.

1.17 The covariance function

The basic problem is that the required covariance function cannot be determined directly from measurements on only one tower because correlation information in the cross-wind direction is obviously missing. The multi-tower TOLCAT project of the U. S. Air Force is an important step in obtaining the necessary empirical data.

It was shown that the response spectra, as defined for a discrete domain, could be obtained if the covariance tensor $R_{ij}(\underset{\sim}{x},t; \underset{\sim}{x}',t')$ [or for simple cases, $R_u(\underset{\sim}{x},t; \underset{\sim}{x}',t')$] were known. This is the same point reached in a thorough study of the dependence of the response of V/STOL aircraft on atmospheric forcing by Skelton (1968). The general lack of either theoretical or empirical knowledge about this important function for the case of atmospheric turbulence was discussed by Skelton. He proposed a model based on considerations related to Taylor's hypothesis which served to permit explicit response calculations.

1.18 Conclusion

Development of methodology for predicting the in-flight response statistics of both launch vehicles and V/STOL aircraft is a much more

difficult task than the equivalent problem for conventional aircraft --
and even the simpler aircraft problem has not been completely resolved.

At the heart of the difficulty is the fact that many of the
powerful simplifying assumptions used in theoretical studies of both
turbulent motion and response of randomly forced systems are not
applicable. Thus, the mathematical methods are more complex, and the
dependence of the results upon the precise nature of the atmospheric
forcing appears to be critical.

However, the main lines the investigation must take seem clear,
and success will be possible if the wells of perseverance do not run
dry.

Acknowledgments

References

Cramér, H., and M. R. Leadbetter, 1967: *Stationary and Related
Stochastic Processes*, John Wiley & Sons, Inc., New York.

Crandall, S. H., 1963: Zero crossings, peaks, and other statistical
measures of random responses. *J. Acoust. Soc. Am.*, 35,
1693-1699.

Dutton, J. A., 1968: Broadening horizons in prediction of the effects
of atmospheric turbulence on aeronautical systems, AIAA Paper
68-1065. To appear in *Progress in Aeronautical Sciences*,
Pergamon Press.

Dutton, J. A., D. G. Deaven and G. J. Thompson, 1969: The probabilistic structure of clear air turbulence -- Some observational results and implications. To appear in *Proceedings of the Boeing Conference on Clear Air Turbulence,* Plenum Press.

Kutzbach, J. E., 1967: Empirical eigenvectors of sea-level pressure, surface temperature, and precipitation complexes over North America, J. Appl. Meteor., 6, 791-802.

Loéve, M., 1963: *Probability Theory*, D. Van Nostrand Co., Inc., Princeton, N. J.

Lorenz, E. N., 1956: Empirical orthogonal functions and statistical weather prediction. Scientific Report No. 1 under Contract AF19(604)1566, AFCRC-TN-57-256, AD110268.

Lumley, J. L., 1965: The structure of inhomogeneous turbulent flows. *Atmospheric Turbulence and Radio Propagation,* A. M. Yaglom and V. I. Tatarsky, eds., Publishing House Nauka, Moscow.

Rice, S. O., 1939: The distribution of maxima of a random curve. Amer. J. Math., 61, 409-416.

Rice, S. O., 1944-45: Mathematical analysis of random noise, Bell System Tech. J., 23, 282-332 and 24, 46-156.

Skelton, G. B., 1968: Investigation of the effects of gusts on V/STOL craft in transition and hover. Flight Dynamics Laboratory Technical Report 68-85, Wright-Patterson AFB, Ohio.

II. ANALYSIS OF MEAN WIND PROFILES

Alfred K. Blackadar and Anton Chaplin

2.1 Aerodynamic roughness of the site

The aerodynamic roughness z_o of the surface is a basic parameter with respect to many aspects of the flow in the surface layers. Its determination is most readily made by a careful study of the mean flow near the ground because the aerodynamic theory of this flow has received the greatest amount of study and has been tested under the widest variety of environmental situations.

The best indicators of surface roughness are the winds at the lowest levels on the tower. At these levels the complications arising from buoyancy, change of stress with height, and possible changes of roughness upstream have relatively minor effects.

Even cursory inspection of the site, or photographs thereof, suggests that the roughness, as revealed by wind profiles, should vary considerably with wind direction. An analysis of the measured values by wind direction is described in this section. In the remaining portions of this chapter studies to assess the effects of inhomogeneous terrain and height decrease of stress are briefly discussed.

The procedure by which roughness lengths were derived is the following.

(1) The mean wind profiles in m sec^{-1} were plotted for each run on 5 cycle semi-logarithmic graph paper.

(2) The mean temperature profiles in °F were plotted for each run on linear graph paper.

(3) The temperature at 30 meters was determined from (2) and the gradient Richardson number at 23 meters for each case was calculated using Eq. (2.1)

(2.1)
$$Ri_{23} = \frac{115(\theta_{30} - \theta_{18})}{\overline{T}(u_{30} - u_{18})^2}$$

where θ and u refer to the potential temperature and mean wind speed at the level indicated by subscript, and $\overline{T}$ is the mean absolute temperature between the two levels.

(4) Each non-stable wind profile was corrected for stability according to the equation

$$(2.2) \qquad u = \frac{u_{*0}}{k} \left[\ell n \, \frac{z}{z_0} \; - \; \psi(Ri) \right]$$

where u is the mean wind speed at height z, k is von Kármán's constant with numerical value 0.4, ψ is a universal function of the local Richardson number, and u_{*0} is the surface friction velocity. It was assumed that Ri is a linear function of height and only the lowest two heights, 18 and 30 meters, were used to determine the slope of the new profile.

(5) From (4) the values of z_0 and u_{*0} were directly obtained and the complete results are printed in Table 2.1. Also see Fig. 2.1.

(6) After carefully inspecting Table 2.1 and a topographical map of the KSC area we divided the results into sectors that visually appeared to have similar roughness elements.

(7) The wind profiles referred to in (6) were further divided into near-neutral and unstable cases indicated by N and U. See Table 2.2. Note: Stable cases were not analyzed.

(8) For each category in Table 2.2 a composite wind profile was determined from which z_0 and u_{*0} were obtained in the same manner as for the individual wind profiles. The results are given in Table 2.3 and Fig. 2.2.

The entire procedure enumerated above was carried through twice. Some noteworthy conclusions have been deduced from the analysis with the aid of the tables and graphs and are presented as follows:
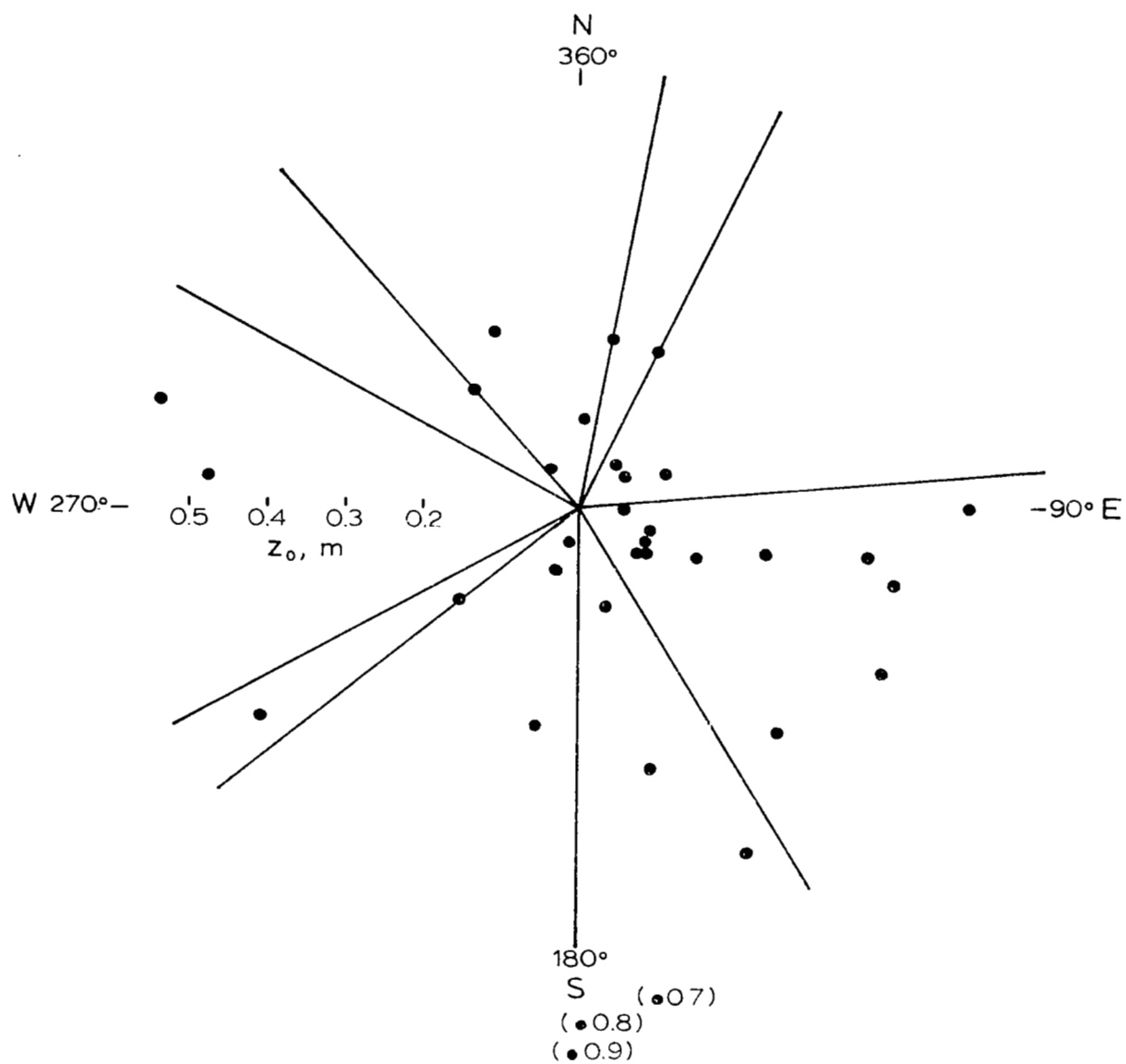
Figure 2.1 Roughness length computed from the wind profile of
individual runs as function of wind direction.

Table 2.1 Richardson number at 23 m, roughness length and friction velocity computed for individual runs. The subscripts C and F refer to values computed by Chaplin and Fichtl, respectively. Wind direction given as average in first 30 m. Wind speed given at the height of 10 z_o.

Run No.	Wind Direction degrees	Ri_C	Ri_F	z_{oC} m	z_{oF} m	Wind Speed m sec^{-1}	u_{*o} m sec^{-1}
013	10	-0.04	-0.06	0.23	0.22	6.7	1.20
020	320	-0.83	-1.33	0.21	0.21	2.9	0.49
029	85	+0.14	-0.19	-	-	-	-
030	70	-0.16	-0.19	0.12	0.09	4.4	0.76
057	105	-0.18	-0.19	0.25	0.28	4.9	0.85
067	55	-0.32	-0.52	0.07	0.10	3.3	0.57
070	130	-0.39	-0.58	0.10	0.12	3.2	0.55
075	155	-0.20	-0.32	0.52	0.52	4.0	0.70
078	285	-0.04	-0.08	0.56	0.88	4.2	0.72
082	5	-0.12	-0.18	0.12	0.20	4.2	0.73
091	275	-0.17	-0.31	0.48	0.59	4.0	0.69
095	170	-0.05	-0.08	0.70	-	5.0	0.87
096	165	-0.19	-0.27	0.37	0.48	4.5	0.78
098	25	-0.30	-0.46	0.23	0.26	3.5	0.61
101	105	-0.23	-0.41	0.42	-	2.6	0.45
107	200	+0.08	+0.10	-	-	-	-
110	325	-0.57	-0.51	0.06	0.06	2.9	0.51
118	90	-0.33	-0.40	0.50	0.47	3.4	0.58
121	335	-1.01	-1.42	0.26	0.25	2.6	0.45
133	140	-0.14	-0.14	0.40	0.38	2.8	0.49
136	165	-0.24	-0.67	0.14	0.52	2.0	0.34
137	180	bad	-	-	-	-	-
138	95	-2.36	-2.85	0.06	0.08	1.8	0.31
141	40	-2.32	-1.95	0.07	0.17	1.9	0.33
142	210	+0.08	+0.08	-	0.08	-	-

143	220	+0.11	+0.13	–	–	–	–
144	220	+0.14	+0.16	–	–	–	–
149	125	−0.60	−1.39	0.11	0.08	2.3	0.40
150	125	−0.36	−1.04	0.04	0.08	2.3	0.40
151	90	−9.75	−13.58	–	–	–	–
152	60	–	–	–	–	–	–
155	180	−0.31	−0.63	0.90	–	2.1	0.36
156	130	+0.02	+0.08	–	–	–	–
159	190	−0.66	−1.68	0.30	0.24	2.5	0.36
160	230	−0.92	−2.15	0.20	0.14	2.0	0.35
162	180	−0.20	−0.46	0.80	0.53	3.0	0.52
163	110	−0.33	−0.77	0.10	0.42	1.8	0.34
164	355	bad	–	–	–	–	–
165	100	−0.21	−0.25	0.38	0.48	3.6	0.62
167	120	−0.27	−0.34	0.45	–	1.6	0.28
170	130	−5.08	−7.62	–	–	–	–
172	120	−0.78	−1.17	0.10	0.19	2.2	0.38
173	200	−1.13	−1.56	0.09	0.27	2.0	0.35
174	235	−0.68	−1.74	0.50	–	1.4	0.24
176	115	−1.08	−2.27	0.17	0.21	1.6	0.28

Table 2.2 Richardson number at 23 m, roughness length and friction velocity of individual runs tabulated in wind-direction groups. N denotes near-neutral runs, U unstable runs. Wind speed given at 18 and 150 m.

Stability	Run No.	Ri	z_o m	Wind Direction degrees	Wind Speed m sec^{-1}	u_{*o} m sec^{-1}
				Group O. Wind Direction (320°-10°)		
N	013	-0.04	0.23	10	12.1-16.8	1.20
N	082	-0.12	0.12	5	8.5-10.4	0.73
U	110	-0.57	0.06	325	6.1- 7.2	0.51
U	121	-1.01	0.26	335	3.8- 5.0	0.45
U	020	-0.83	0.21	320	4.4- 5.4	0.49
				Group I. Wind Direction (25°-85°)		
N	030	-0.16	0.12	70	9.0-12.6	0.76
U	067	-0.32	0.07	55	7.2- 8.4	0.57
U	098	-0.30	0.23	25	6.0- 7.0	0.61
				Group II. Wind Direction (85°-150°)		
N	057	-0.18	0.25	105	8.0-11.3	0.85
N	133	-0.14	0.40	140	4.3- 5.7	0.49
U	070	-0.39	0.10	130	6.4- 8.3	0.55
U	101	-0.23	0.42	105	3.6- 4.9	0.45
U	118	-0.33	0.50	90	4.4- 5.3	0.58
U	149	-0.60	0.11	125	4.5- 4.8	0.40
U	150	-0.36	0.04	125	5.5- 6.0	0.40
U	163	-0.33	0.10	110	3.4- 4.0	0.34
U	165	-0.21	0.38	100	5.2- 7.2	0.62
U	167	-0.27	0.45	120	2.2- 3.7	0.28
U	172	-0.78	0.10	120	4.5- 5.0	0.38
U	176	-1.08	0.17	115	2.8- 3.3	0.28

Groups I & II. Wind Direction (25°-150°)

N	030	-0.16	0.12	70	9.0-12.6	0.76
N	057	-0.18	0.25	105	8.0-11.3	0.85
N	133	-0.14	0.40	140	4.3- 5.7	0.49
U	067	-0.32	0.07	55	7.2- 8.4	0.57
U	098	-0.30	0.23	25	6.0- 7.0	0.61
U	070	-0.39	0.10	130	6.4- 8.3	0.55
U	101	-0.23	0.42	105	3.6- 4.9	0.45
U	118	-0.33	0.50	90	4.4- 5.3	0.58
U	149	-0.60	0.11	125	4.5- 4.8	0.40
U	150	-0.36	0.04	125	5.5- 6.0	0.40
U	163	-0.33	0.10	110	3.4- 4.0	0.34
U	165	-0.21	0.38	100	5.2- 7.2	0.62
U	167	-0.27	0.45	120	2.2- 3.7	0.28
U	172	-0.78	0.10	120	4.5- 5.0	0.38
U	176	-1.08	0.17	115	2.8- 3.3	0.28

Group III. Wind Direction (150°-180°)

N	095	-0.05	0.70	170	6.6- 8.9	0.87
U	075	-0.20	0.52	155	5.5- 7.4	0.70
U	096	-0.19	0.37	165	6.9- 8.7	0.78
U	136	-0.24	0.14	165	3.6- 6.2	0.34
U	155	-0.31	0.90	180	2.4- 3.6	0.36
U	162	-0.20	0.80	180	3.7- 5.0	0.52

Group IV. Wind Direction (180°-230°)

U	159	-0.66	0.30	190	3.2- 4.0	0.36
U	160	-0.92	0.20	230	3.2- 3.9	0.35
U	173	-1.13	0.09	200	3.8- 4.5	0.35
U	174	-0.68	0.50	235	1.7- 2.4	0.24

Group V. Wind Direction (240°-300°)

N	078	-0.04	0.56	285	6.0- 9.0	0.72
U	091	-0.17	0.48	275	5.6- 7.8	0.69

Table 2.3. Characteristics of composite groups. The subscripts C and F refer to values computed by Chaplin and Fichtl, respectively. Wind speed given as average between 18 and 150 m.

Designation	Ri at 23 m	z_{oC} m	u_* m sec^{-1}	Mean Direction degrees	Average Speed m sec^{-1}	z_{oF} m	R_θ	R_u	R_θ/R_u
O:N	−0.080	0.14	0.90	345	12.2	0.23	1.44	0.79	1.823
O:U	−0.803	0.06	0.40	−	5.3	−	0.93	1.90	0.489
I:N	−0.160	0.12	0.77	55	10.8	0.23	0.94	1.67	0.563
I:U	−0.310	0.06	0.51	−	7.1	−	0.96	0.78	1.231
II:N	−0.160	0.27	0.65	120	7.5	0.23	0.94	1.58	0.595
II:U	−0.458	0.26	0.47	−	4.7	−	1.39	0.70	1.986
I & II:N	−0.160	0.21	0.70	90	8.6	0.23	0.94	1.48	0.635
I & II:U	−0.433	0.12	0.43	−	5.1	−	1.31	0.71	1.845
III:N	−0.050	0.70	0.87	165	7.8	0.51	2.69	0.91	2.956
III:U	−0.228	0.42	0.53	−	5.3	−	1.70	1.18	1.441
IV:N	−	−	−	205	−	0.23	−	−	−
IV:U	−0.848	0.10	0.27	−	3.3	−	1.76	1.75	1.006
V:N	−0.040	0.56	0.72	270	7.5	0.65	1.50	1.33	1.128
V:U	−0.170	0.48	0.69	−	6.8	−	1.48	1.33	1.113
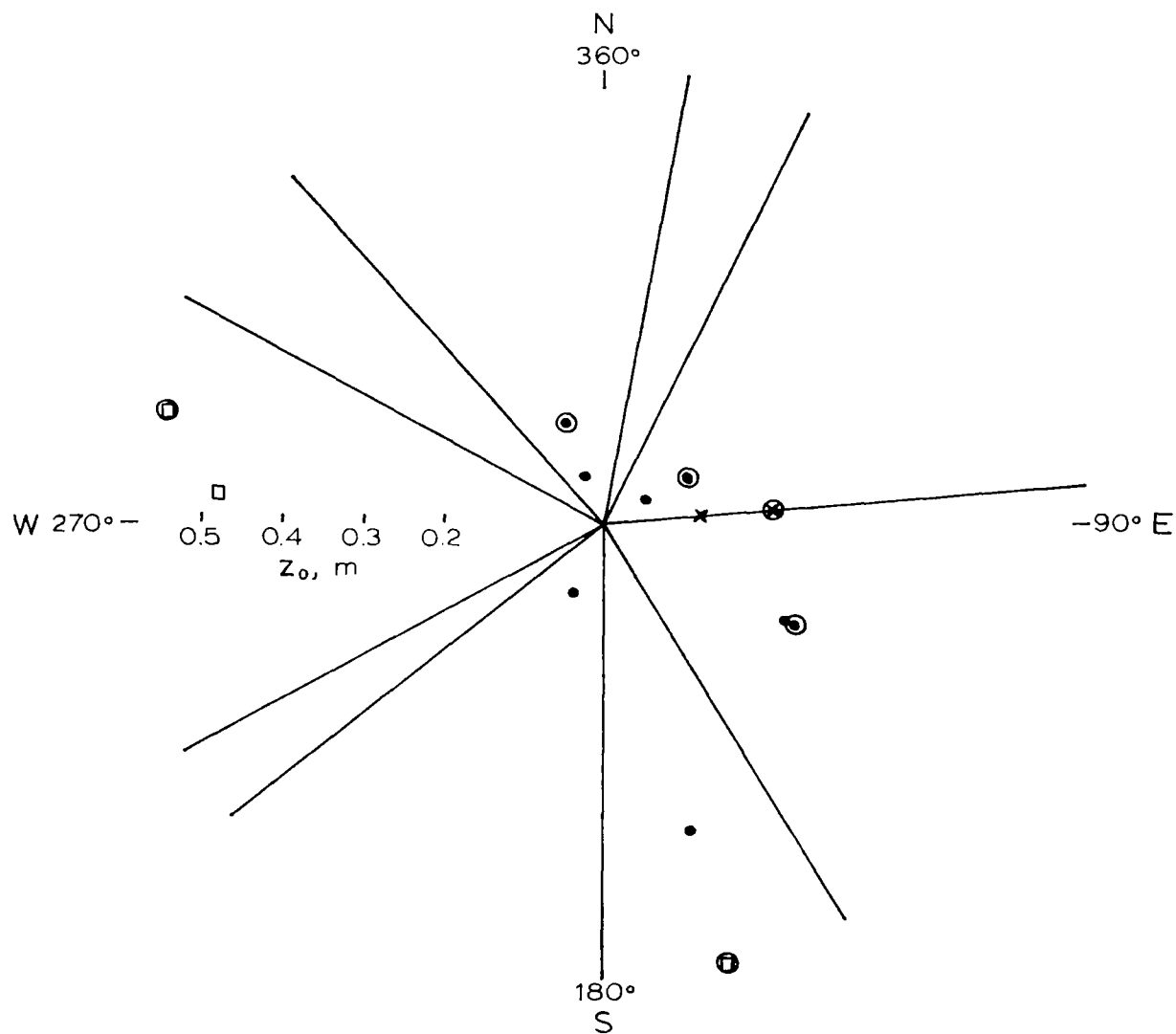
Figure 2.2   Roughness length computed from the average wind profile
of wind-direction groups as function of wind direction.
Squares denote single runs, dots composite runs.   Circles
represent neutral cases.

(1) The roughness length determined from a near-neutral wind
profile is more reliable than one obtained from a very
unstable profile because in the latter case the uncertainty
in the gradient Richardson number and hence in $\psi(Ri)$ becomes
quite large.

(2) Although there is some scatter of z_o in every sector as
revealed in Fig. 2.1, Tables 2.2 and 2.3 indicate that the
roughness length at KSC is independent of stability and
wind speed.

(3) The values of z_o computed by Fichtl (1968) on a computer and
those computed by Chaplin without the aid of a computer are
most compatible.

(4) Large variations in the value of the gradient Richardson
number nevertheless yield similar values of roughness length
as revealed in Table 2.1.

(5) A value of z_o determined from a composite wind profile is
more realistic than a value of z_o determined from an
individual wind profile because the effects of errors
attributed to sensors and calculation techniques are
minimized when one uses an "average" wind profile.

In order to learn more about the transfer mechanisms in the lowest
layers of the atmosphere one may study profiles of temperature and wind.
The stress and heat flux are related to the wind shear and lapse rate by
the equations

(2.3) $\tau = \rho K_M \partial u / \partial z$

(2.4) $H = -\rho c_p K_H \partial \theta / \partial z$

where τ is the tangential eddy stress, H the upward eddy heat flux, ρ the
density; K_M and K_H are the exchange coefficients for momentum and heat,
respectively.

If both the heat and momentum fluxes are "constant" in the first 60 meters then one may write

(2.5) $$\frac{K_{H2}/K_{M2}}{K_{H1}/K_{M1}} = \frac{R_\theta}{R_u}$$

where $R_\theta = \dfrac{\theta_{60} - \theta_{30}}{\theta_{30} - \theta_{18}}$ and $R_u = \dfrac{u_{60} - u_{30}}{u_{30} - u_{18}}$

For near-neutral conditions $K_{H1}/K_{M1} \simeq 1$ and thus $R_\theta/R_u \simeq K_{H2}/K_{M2}$. Qualitatively, even for unstable conditions, as a first approximation we may use the preceding relationship. The results are given in Table 2.3; they are not conclusive, but composite cases O:N, III:N, and V:N do suggest that K_H is greater than K_M, in agreement with previous investigations. For non-neutral conditions it is probably not proper to form the ratio R_θ/R_u because the fluxes are not even approximately constant.

2.2 Approximate theory of diabatic wind profiles up to 150 m

The 150-m tower at Cape Kennedy is sufficiently high to make it necessary to abandon the assumption of constancy of stress on which the diabatic wind profile theory is based. In order to analyze wind profiles observed on this tower it is necessary to turn to more comprehensive theories of the planetary layer. Several of these theories are available for neutral stratification, Blackadar (1962, 1965), Lettau (1962) and Appleby and Ohmstede (1964), and two have been proposed for unstable stratification by Blackadar and Ching (1965) and Bobileva et al. (1965). Of the latter two, only Blackadar and Ching's model has been integrated. These theories are not suitable for curve fitting to observed data because only numerical solutions have been obtained.

A method of approximating these numerical profiles has been proposed by Blackadar and Tennekes (1968) and by using the principles

58

of asymptotic similarity a method for fitting neutral wind profiles has
been given. The application of this approximation in diabatic
stratification can now be attempted, and this will be described in this
section.

The basic assumption of the method is that the mean wind
direction does not usually change significantly with height within the
lowest 150 meters. The validity of this approximation is demonstrated
by all of the numerical models that have been given, as well as by
numerous observed wind profiles. This assumption serves to a much
greater height than the constancy of stress, which often shows a 30 percent
decrease in the lowest 150 m. If we now define the x-axis to be the
direction of the wind near the ground, the first equation of motion, for
steady-state mean conditions becomes, simply

$$(2.6) \qquad \frac{d}{dz} K_M \frac{du}{dz} = fv_g$$

where v_g is the y-component of the geostrophic wind and f is the Coriolis
parameter. This may be integrated with respect to height to give

$$(2.7) \qquad K_M \frac{du}{dz} = u_{*_o}^2 (1 - \frac{z}{Y})$$

where u_{*_o} is the surface value of the friction velocity and Y satisfies

$$(2.8) \qquad Y = - \frac{u_{*_o}^2}{fv_g}$$

In order to determine v_g we may impose the result of the theory of
asymptotic similarity

$$(2.9) \qquad \frac{v_g}{u_{*_o}} = \frac{A(\sigma)}{k}$$

where σ is defined as u_{*_o}/fL_o. It may be regarded as a bulk Richardson
number for the planetary boundary layer. This result was first predicted

by Bobileva et al. (1965) in a specialized way. It has since been shown
by Blackadar and Tennekes (1968) that this result is more generally
valid. Under neutral stratification ($\sigma = 0$), the value of A has been
shown to be about 5. An empirical determination of $A(\sigma)$ has recently
been given by Zilitinkevich and Chalikov (1968), but this is based only
on data for one station. Priestley has also made very recent determina-
tions of the function $A(\sigma)$, but these have not been available for use.
Accordingly we put

$$(2.10) \qquad Y = ku_{*_o}/fA(\sigma)$$

In order to integrate (2.7) to get the wind distribution, it is
necessary to parameterize K_M in a suitable way. Panofsky (1961) has
shown that in the constant-stress layer K_M can be predicted by the relation

$$(2.11) \qquad K_M = [u_*^2 \frac{du}{dz} + \frac{\gamma gH}{c_p \rho T}]^{1/3} \ell^{4/3}$$

where γ is an empirical coefficient, H is the surface heat flux, and ℓ
is kz. To adapt this expression for use through a non-constant stress
layer, it is necessary to replace u_*^2 by $K_M \, du/dz$ and to replace $\ell = kz$
by

$$(2.12) \qquad \ell = kz/(1 + \frac{kz}{\lambda_B}) \, , \qquad \text{with} \quad \lambda_B = .0063 \frac{u_{*_o}}{f}$$

which was found to be necessary to describe the flow in the planetary
boundary layer under neutral conditions (Blackadar, 1965).

It may be asked whether ℓ should depend on the Richardson number
in some way. Such a procedure is not appropriate for two reasons. First,
it appears that near the boundary the significant scale is distance from
the boundary, while in the planetary boundary layer this is always u_{*_o}/f,
a fact which follows from the equations of motion without any regard
for considerations of stability. Secondly, it can easily be shown that

within the constant stress layer a variation of ℓ with Richardson number is equivalent to a change of the value of γ. The value of γ that we shall use, 15 (18 when H is replaced by $-c_p \rho K_M \partial\theta/\partial z$), has been established on the assumption that ℓ is independent of Richardson number. Thus it is appropriate to follow the same procedure in extending the surface layer. Thus, upon extending the definitions of the quantities in Eq. (2.11) and using (2.3) and (2.12) we find

$$(2.13) \qquad K_M = \left[K_M (\frac{du}{dz})^2 - \frac{\gamma u_{*o}^3}{kL_o} \right]^{1/3} \left[\frac{kz}{(1 + \frac{kz}{\lambda_B})} \right]^{4/3}$$

where L_o is the surface Monin length

$$(2.14) \qquad L_o = - \frac{c_p \rho T u_{*o}^3}{kgH}$$

and H is the turbulent heat flux at the surface. Here and in the subsequent discussion we do not take into account any effect of the change of heat flux in the vertical. There appear to be no experimental reasons compelling that such a variation of heat flux needs to be included in wind profile theories, and it is included for simplicity. Further assessment of this effect is needed.

It will be useful here to replace du/dz in (2.7) and (2.13) by an equivalent function ϕ, the so-called universal function defined by

$$(2.15) \qquad \phi = \frac{kz}{u_{*o}} \frac{du}{dz}$$

with the understanding that u_{*o} is to be the value at the surface, as heretofore. Finally we eliminate K_M between Eqs. (2.7) and (2.13) and obtain the equation

$$(2.16) \qquad \phi^4 - \frac{\gamma z}{L_o(1 - \frac{z}{Y})} \phi^3 = (1 - \frac{z}{Y})^2 (1 + \frac{63zf}{u_{*o}})^4$$

which may be regarded as the appropriate generalization of the KEYPS
equation for the layer of constant wind direction.

Panofsky (1963) has shown that for the constant stress layer,
the KEYPS equation has a solution of the form

$$(2.17) \qquad \frac{u}{u_{*o}} = \frac{1}{k} \left[\ell n \frac{z}{z_o} - \psi_1 \left(\frac{z}{L_o} \right) \right]$$

and has given a graph of the function $\psi_1(z/L_o)$. The author has shown
elsewhere (Blackadar and Tennekes, 1968) that for neutral stratification
in the constant wind-direction layer, the wind profile may be approximated
by the equation

$$(2.18) \qquad \frac{u}{u_{*o}} = \frac{1}{k} \left[\ell n \frac{z}{z_o} - \psi_2 \left(\frac{zf}{u_{*o}} \right) \right]$$

and has given graphs of the function $\psi_2 \left(\frac{zf}{u_{*o}} \right)$ for two of the integrated
planetary boundary layer models. For the general diabatic case, the
solution will be represented by the form

$$(2.19) \qquad \frac{u}{u_{*o}} = \frac{1}{k} \left[\ell n \frac{z}{z_o} - \psi_1 \left(\frac{z}{L_o} \right) - \psi_2 (Z, \sigma) \right]$$

where Z stands for zf/u_{*o}, and we shall seek those conditions for which
this simple form is valid. One of the questions to be determined is the
form of the unknown function ψ_2. Since the form can be predicted for the
neutral case, it is desirable to know to what extent the variation of ψ_2
with stability could be ignored, so as to permit the correction for
stress variations to be applied independently of the correction for
stability.

Let us now define the following quantities.

$$(2.20) \qquad b = \frac{u_{*o}}{fY} = \frac{A(\sigma)}{k} \quad ; \quad a = \frac{ku_{*o}}{f \lambda_b} \simeq 63$$

Differentiation of (2.19) with respect to z gives the relation

$$(2.21) \qquad \phi = \phi_1 \left(\frac{z}{L_o}\right) + \phi_2 (Z,\sigma)$$

where

$$(2.22) \qquad \phi_1 = 1 - \frac{z}{L_o} \psi_1' = 1 - \sigma Z \psi_1'$$

where $\psi_1' = d\psi_1/d(z/L_o)$, and

$$(2.23) \qquad \phi_2 = - Z\psi_2'$$

where $\psi_2' = \partial\psi_2/\partial Z$. Furthermore, ϕ_1 satisfies the KEYPS equation

$$(2.23a) \qquad \phi_1^{\;4} - \frac{\gamma z}{L_o} \phi_1^{\;3} = 1$$

We now expand Eq. (2.16) in powers of Z, retaining terms in Z^2 or lower,

$$(2.24) \qquad 4\phi_1^{\;3}\phi_2 + 6\phi_2^{\;2} - \gamma\sigma Z(3\phi_1^{\;2}\phi_2) - \gamma\sigma b Z^2 =$$

$$(4a - 2b)Z + (b^2 - 8ab + 6a^2)Z^2$$

Use has been made of the fact that ϕ_1 satisfies (2.23a), and that $(\phi_1 - 1)$ and ϕ_2 are of order Z at the lowest.

Upon substitution of (2.23) we obtain

$$(2.25) \qquad -4\psi_2' + 3\sigma Z\psi_1'\psi_2' + 6Z\psi_2'^{\;2} + 3\gamma Z\psi_2' =$$

$$(4a - b) + (\gamma\sigma b + b^2 - 8ab + 6a^2)Z$$

To a first approximation (equivalent to satisfying the general equation in ϕ to first order in Z only) we obtain

$$(2.26) \qquad \psi_2 = - (a - \frac{1}{2} b)Z = - (63 - 6)Z = - 57Z$$

Except for the slight dependence of b on σ, this approximation to ψ_2 is independent of σ, and the corrections for stability and height variation of stress can be made independently. When, however, the height becomes so large that second or higher order terms in Z have to be included, ψ_2 depends on σ (both directly and indirectly through ψ_1), and the two corrections are no longer independent of each other.

It should be noted that, although the value of b depends to some extent on stability, the value of ψ_2/Z to this approximation is not sensitive to stability variations. Since the function $A(\sigma)$ is not well known, the dependence of b on σ will be ignored for the present, and will not have any significant effect.

The object of wind profile equations such as (2.19) is to furnish a means of calculating the significant parameters z_o and u_{*o} which are needed for the parameterization and prediction of other wind statistics. Therefore, it is necessary to consider how wind profile observations can be applied to (2.19) for calculating z_o and u_{*o}. It is also important to determine what errors are inherent in the parameters z_o' and u_*' determined by constant-stress layer analysis through the use of the more common equation

$$(2.27) \qquad u = \frac{u_*'}{k} \left[\ell n \frac{z}{z_o'} - \psi_1 \left(\frac{z}{L_o} \right) \right]$$

The determination of z_o and u_{*o} is generally most accurately done from the two or three lowest levels of observation. Since this is the case, the approximations used in this section are especially appropriate for the determination of these parameters. This analysis is greatly

facilitated by a fortunate coincidence. If we consider the product $-\psi_2 u_{*o}/k$ which in (2.19) is seen to be the correction to u resulting from the variation of stress, we find it is independent of u_{*o} and z_o. This is fortunate, since it permits the effect to be removed before the values of the parameters are known. Thus, by the use of (2.19) and (2.26), we have

$$(2.28) \qquad u_c = (u - \frac{57fz}{k}) = \frac{u_{*o}}{k} \left[\ln \frac{z}{z_o'} - \psi_1(\frac{z}{L_o}) \right]$$

and we see that u_c is related to the true values of u_{*o} and z_o by the same Eq. (2.27) as has usually been applied in the constant stress technique. Therefore, to obtain the true values of u_{*o} and z_o one simply subtracts 57fz/k from each observed wind speed and proceeds by Panofsky's technique to derive the parameters.

When values of z_o' have been found by previous analysis, as is the case in the Cape Kennedy analysis, the corrected values of z_o can be found without reanalysis.

If we eliminate ℓn z between (2.19) and (2.27) we obtain

$$(2.29) \qquad \ln \frac{z_o'}{z_o} = \frac{ku}{u_{*o}} (1 - \frac{u_{*o}}{u_*'}) - \frac{57fz}{u_{*o}}$$

This equation must be satisfied at all levels. It yields two equations for the determination of z_o and u_{*o} if we apply it at the same two levels that have been used for the determination of z_o' and u_*'. Calling these levels 1 and 2, we can then eliminate ℓn (z_o'/z_o) from the two equations and solve for u_{*o}/u_*'

$$(2.30) \qquad \frac{u_{*o}}{u_*'} = 1 - \frac{57f}{k} \frac{z_2 - z_1}{u_2 - u_1}$$

Having thus obtained u_{*o} from the previous estimate u_*', one may then apply (2.29) at either level to get z_o from z_o'.

The values of z_o and u_{*o} that had been determined previously, as listed in Report 8 were subjected to a redetermination in accordance with these techniques, and the comparisons are shown in Table 2.4. The average of the corrected values of z_o is 32 percent of the original values, while the average of the corrected values of u_{*o} is 68 percent of the uncorrected values. On the basis of other evidence to be given later, it appears that corrections such as these are required, but may be somewhat too large in magnitude.

References

Appleby, J. R. and W. D. Ohmstede, 1964: Numerical solution of the distribution of wind and turbulence in the planetary boundary layer. Meteor. Res. Note, No. 8, Meteor. Dept., Fort Huachuca, Arizona, 47 pp.

Blackadar, A. K., 1962: The vertical distribution of wind and turbulent exchange in a neutral atmosphere. J. Geophys. Res., 67, 3095-3102.

Blackadar, A. K., 1965: A single-layer theory of the vertical distribution of wind in a baroclinic neutral atmospheric boundary layer. Pp. 1-22 in Final Report Contract No. AF(604)-6641, The Pennsylvania State Univ., 140 pp.

Blackadar, A. K. and J. K. S. Ching, 1965: Wind distribution in a steady state planetary boundary layer of the atmosphere with upward turbulent heat flux. Pp. 23-48 in Final Report Contract No. AF(604)-6641, The Pennsylvania State Univ., 140 pp.

Blackadar, A. K., H. A. Panofsky, P. E. Glass and J. F. Boogaard, 1967: Determination of the effect of roughness change on the wind profile. Physics Fluids Suppl., 209-211.

Blackadar, A. K. and H. Tennekes, 1968: Theory of the steady-state wind distribution over homogeneous terrain. Pp. 1-18 in the Second ,Annual Report ECOM-01388-1, The Pennsylvania State Univ., 38 pp.

Bobileva, I. M., S. S. Zilitinkevich and D. L. Laikhtman, 1965: Turbulent exchange in the thermally-stratified planetary boundary layer of the atmosphere. Acad. Sci. USSR, International Colloquium on the Fine-scale Structure of the Atmosphere, Moscow, 1965.

Table 2.4 Corrected wind profile parameters.

Run No.	z_o' (m)	z_o (m)	u_*' (m sec^{-1})	u_{*o} (m sec^{-1})
013	0.23	0.16	1.20	1.08
020	0.21	0.019	0.49	0.28
030	0.12	0.046	0.76	0.62
057	0.25	0.13	0.85	0.71
067	0.07	0.013	0.57	0.42
070	0.10	0.17	0.55	0.39
075	0.52	0.25	0.70	0.55
078	0.56	0.37	0.72	0.62
082	0.12	0.054	0.73	0.61
091	0.48	0.24	0.69	0.55
095	0.70	0.49	0.87	0.76
096	0.37	0.20	0.78	0.65
098	0.23	0.070	0.61	0.45
101	0.42	0.19	0.45	0..35
110	0.06	0.005	0.51	0.33
118	0.50	(0)	0.58	0.04
121	0.26	0.015	0.45	0.23
133	0.40	0.14	0.49	0.36
136	0.14	0.18	0.34	0.22
149	0.11	(0)	0.40	0.12
150	0.04	(0)	0.40	0.23
155	0.90	0.23	0.36	0.22
159	0.30	0.003	0.36	0.15
160	0.20	(0)	0.35	0.11
162	0.80	0.24	0.52	0.35
163	0.10	0.008	0.34	0.20
165	0.38	0.167	0.62	0.48
167	0.45	0.104	0.28	0.18
172	0.10	0.005	0.38	0.22
173	0.09	0.003	0.35	0.18
174	0.50	0.017	0.24	0.10
176	0.17	(0)	0.28	0.07

References (continued)

Fichtl, G. H., 1968: An analysis of the roughness length associated with the NASA 150-meter tower. Tech. Mem. X-53690.

Lettau, H. H., 1962: Theoretical wind spirals in the boundary layer of a barotropic atmosphere. Beiträge zur Phys. der Atmosphäre, 35, 195-212.

Panofsky, H. A., 1961: An alternative derivation of the diabatic wind profile. Quart. J. R. Met. Soc., 87, 109-110.

Panofsky, H. A., 1963: Determination of stress from wind and temperature measurements. Quart. J. R. Met. Soc., 89, 85-94.

Panofsky, H. A. and A. Townsend, 1963: The effect of a change in roughness on the wind profile. XIII General Assembly, IUGG, Berkely, California.

Zilitinkevich, S. S. and D. V. Chalikov, 1968: The laws of resistance and of heat and moisture exchange in the interaction between the atmosphere and an underlying surface. Izv. Akad. Nauk SSSR, Atmos. and Ocean. Phys., 4, 765-772.

III.   SPECTRA OF THE HORIZONTAL WIND COMPONENTS

Hans A. Panofsky

3.1   Treatment of fast-response data

Wind speed and direction were originally recorded every one tenth
of a second, and then averaged in groups of 20 (2-second non-overlapping
means). From these quantities, the sponsor computed longitudinal (u)
components along the vector mean wind, and lateral (v) components at
right angles. Lines of regression were fitted to u and v, and the
deviations from these lines were treated further by the sponsor. The
computations included kurtosis, skewness, standard deviations and spectral
analyses by the Tukey method. Cross spectra between all pairs of levels
(6 levels, 15 pairs) were computed for like velocity components. All
spectrum analysis was made on the basis of 180 lags, so that spectral and
cross spectral estimates extended from periods of 2 seconds to 720 seconds.
Some experimental group averaging was done on the spectra and cospectra.
Spectra and coherence were computer plotted at The Pennsylvania State
University, with results to be discussed later.

3.2   Theory of the inertial range

Even though the conditions for an isotropic inertial subrange can
be satisfied only for wavelengths much smaller than the height above
ground, spectral shapes of the form typical for the inertial range are
observed for the horizontal velocity components for much longer wavelengths
(Busch and Panofsky, 1968). In particular, u-spectra obey the characteristic
-5/3 law up to wavelengths about five times the height (depending somewhat
on stability and height), and even v-spectra follow the same law up to
wavelengths more than twice the height. Therefore, spectral characteristics
of the horizontal wind components can be inferred from simple observations
near the ground through the theory of the inertial range; conversely, the
vertical variation of the dissipation can be found from the spectra. Then

from the energy equation applied close to the ground, we can obtain surface stresses and roughness lengths.

The one-dimensional spectrum in the inertial subrange can be written (see, e.g., Lumley and Panofsky, 1964):

$$(3.1) \qquad S(k) = a\varepsilon^{2/3} k^{-5/3}$$

Here, a represents a constant, which has a value 0.14 for the longitudinal spectrum, and 0.18 for the lateral spectrum; k is the wave number in cycles per unit length; and ε is the dissipation rate of the turbulent kinetic energy. We now define ϕ_ε as $0.4z\varepsilon/u_*^3$, where u_* is the local friction velocity, and apply Taylor's hypothesis.

According to Taylor's hypothesis (see, e.g., Lumley and Panofsky, 1964), local Eulerian fluctuations of a variable with time can be interpreted to be due to variations of that variable along the mean wind direction, being swept past the observer with mean wind speed V. If the fluctuations are just due to a simple translation (frozen wave hypothesis), we can replace the wave number k in Eq. (3.1) by n/V, where n is the frequency. Similarly, the quantity kS(k) (the variance produced by unit logarithmic wave number interval) then equals nS(n), which measures the variance produced in unit logarithmic frequency interval, since $d(\ell n \ n)$ = $d(\ell n \ k)$.

Several experiments, quoted in the above reference, have shown that Taylor's hypothesis is particularly well satisfied at high frequencies. We can then put Eq. (3.1) into the form (subscript zero stands for surface values):

$$(3.2) \qquad \frac{nS(n)}{u_{*_0}^2} = C \ \phi_\varepsilon^{2/3} \ f^{-2/3} \left(\frac{u_*}{u_{*_0}} \right)^2$$

In this equation, f is a nondimensional frequency nz/V, where z is height, and C is a constant equal to 0.26 for longitudinal spectra, and 0.34 for lateral spectra.

We will now define a quantity X by:

$$(3.3) \qquad X = \phi_\varepsilon^{2/3} (u_*/u_{*_0})^2$$

X is the value of $nS(n)/u_{*_0}^2 C$ at $f = 1$. It varies with height, but is independent of frequency. The variation of X with height and stability can be understood from the budget of turbulent kinetic energy:

$$(3.4) \qquad \frac{dE}{dt} = u_*^2 \frac{\partial V}{\partial z} + \frac{gH}{c_p \rho T} + P - D - \varepsilon$$

Here, g is gravity, H the vertical heat flux, c_p the specific heat at constant pressure, ρ the air density, and T the temperature; E is the mean turbulent kinetic energy per unit mass, and D the vertical divergence of the vertical energy flux produced by turbulence, and P is a term describing work done against the fluctuating pressure forces.

We assume that the energy is in equilibrium, that the pressure term is unimportant, and that only the vertical shear of the mean wind is large enough to produce energy; then, the energy equation takes the form (after normalizing by $u_{*_0}^3/0.4z$):

$$(3.5) \qquad X^{3/2} = [\phi(x/L) - z/L - D] \frac{u_*^3}{u_{*_0}}$$

Here, ϕ is the nondimensional wind shear $(0.4z/u_*)(dV/dz)$, and D the normalized energy flux divergence. L is the Monin-Obukhov length $(u_*^3 c_p \rho T)(kgH)$. The behavior of D is uncertain; Busch and Panofsky (1968) have brought together evidence that D is unimportant under all conditions. On the other hand, observations from Brookhaven (Panofsky, 1962) suggest that flux divergence is positive and may cancel z/L in unstable air. But even for these data, D approaches zero in neutral air. In neutral air, therefore, X will most likely tend toward unity as the ground is approached. Recently, Businger (unpublished) has suggested that, in unstable air, D is small above a certain height.

It will be seen that the observed variation of X with height is consistent with the hypothesis that D is unimportant in unstable air (at 30 m and above). We can then write Eq. (3.5) in the form:

$$(3.6) \qquad \left[\left(\frac{u_*}{u_{*o}} \right)^3 \phi(\frac{z}{L}) - \frac{z}{L_o} \right]^{2/3}$$

where L_o is the value of L computed with u_{*o}. The quantity L_o can be obtained from Businger's hypothesis (see Deardorff, 1968) that, at low levels in unstable air,

$$(3.7) \qquad z/L = Ri$$

If we make the reasonable assumption that L is constant below 23 m, we can compute L_o by:

$$(3.8) \qquad L_o = 23m/Ri_{23}$$

where Ri_{23} is the Richardson number at about 23 m, computed from the observed winds and temperatures at 30 m and 18 m.

The quantity z/L_o can be considered as the Richardson number at 23 m, extrapolated upwards linearly to height z. This quantity will also be called Ri_{eff}, the "effective" Richardson number at height z. This quantity is judged to be a better indicator of the relative importance of convective and mechanical turbulence at level z than the measured Richardson number for two reasons: first, both numerator and denominator in Ri become small at high levels so that estimates of Ri become erratic; and second, Ri often changes sign around midtower height, even though the heat flux is still upward and convective turbulence is important. Since the quantity u_*/u_{*o} differs significantly from unity only at considerable height, where, in unstable air, $\phi(z/L)$ is much smaller

numerically than z/L, $(u_*/u_{*_o})^3$ can generally be taken as unity. Only in near neutral air, will the decrease of stress with height cause a gradual decrease of X with height.

If we accept Businger's expression for the diabatic wind profile (see Deardorff, 1968), that

(3.9) $\phi = (1 - 18 \ z/L)^{-1/4}$

we obtain for X:

(3.10) $X = [(1 - 18 \ z/L)^{-1/4} - z/L_o]^{2/3}$

Figure 3.1 is a graph of $\sqrt{X}$ as function of z/L_o in unstable air based on Eq. (3.10), which therefore also represents the variation of the spectra with height at f = 1. Since ϕ is important only for small z, L has been replaced by L_o. Thus, the spectra at f = 1 at first decrease slightly with height, and then increase. For large z/L, X varies as $z^{2/3}$. This is the condition when buoyant energy production is balanced by dissipation.

In neutral air, of course, X will slowly decrease upward from one at the ground. In all cases then, X should approach one as the ground is approached. Since, by definition, the spectra for u and v are of the form:

(3.11) $\dfrac{nS(n)}{u_{*_o}^2} = CXf^{-2/3}$

the above expressions for X make it possible to estimate the spectra to considerable heights, provided that the vertical flux of enthalpy can be taken as a constant, and provided the undetermined factor u_*/u_{*_o} does not become important. At 18 m, Fichtl finds that the observations of ε are better explained by assuming that $\phi_\varepsilon = \phi(z/L)$ implying that buoyant
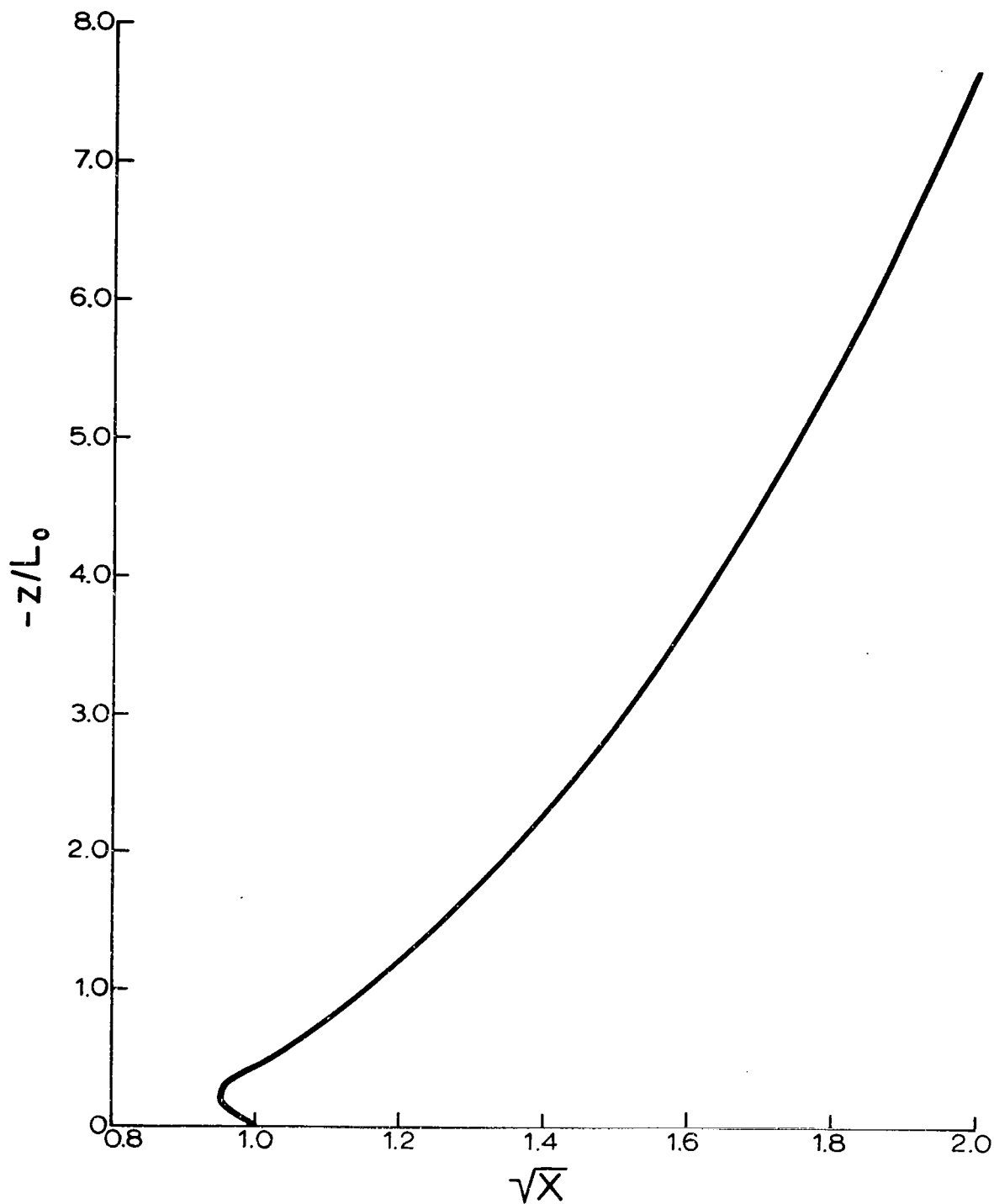
Figure 3.1 Theoretical relation of $\sqrt{X}$ to effective Richardson number.

production and flux divergence cancel here, in agreement with Businger's ideas.

3.3 Observed characteristics of subrange spectra

In practice, some of the above ideas were tested by studying the characteristics of $X = nS(n)/Cu_{*_O}^2$ at $f = 1$. The computation of this quantity required first an estimate of u_{*_O} which was determined from the wind at 18 m, and a roughness length previously determined for that wind direction (Chapter II). Then, X was determined from a computer plot of the spectra on log-log paper, interpolating or extrapolating to $f = 1$.

Figure 3.2 shows the dependence of $X^{1/2}$ on height for the u-component in two typical situations with different stability. In general, such curves are nearly vertical in near-neutral air, and slope toward the upper right in unstable air. The observations above 18 m are well satisfied by Eq. (3.6). However, the value of X at 18 m tends to be significantly lower than a smooth curve drawn through the other data. This characteristic can be understood if, as suggested previously, the flux divergence is important at 18 m but not at the higher levels, as suggested by Businger.

Smooth curves were drawn through the points above 18 m and extrapolated downward to the surface. Here, the value of X goes to one according to Eq. (3.6). The actual values often departed significantly from unity. If we assume that the spectra are of good quality, it follows that the roughness estimated previously from the wind profiles was wrong. This is quite possible, because roughness determinations should be made from wind profiles at levels lower than here available. For this reason, roughness values were recomputed so as to make the limiting value of X at the ground equal to one.

Table 3.1 shows the roughness lengths originally computed as well as the values needed to make X equal to one, at the ground. In many cases, the revised roughness lengths are substantially lower than those determined from the wind profiles. This change is in the right
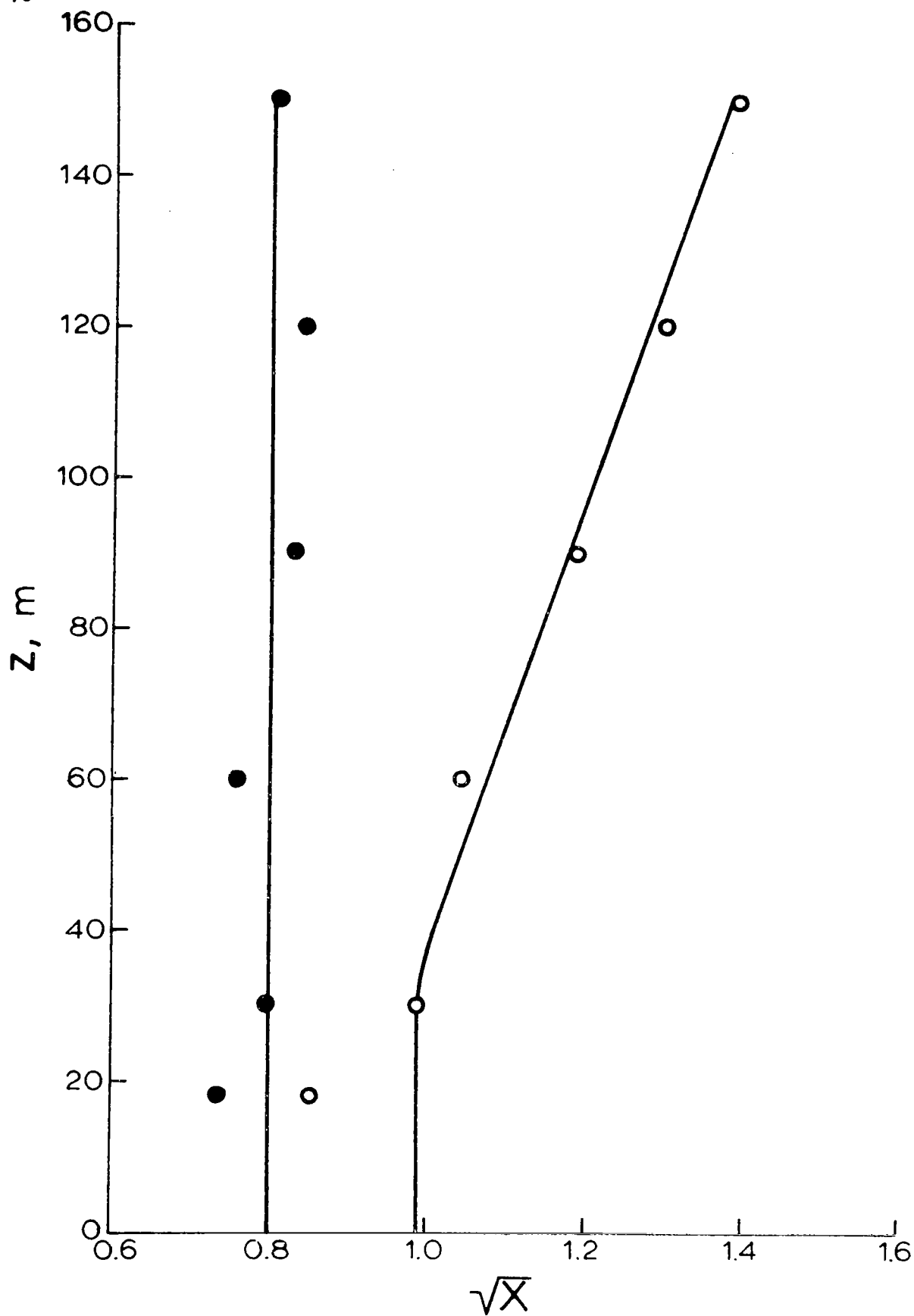
Figure 3.2 Typical relation of $\sqrt{X}$ with height. Dots, neutral ($Ri_{eff} \simeq 0$); circles, unstable ($Ri_{eff} < 0$).

Table 3.1 Roughness lengths computed from wind profiles and spectra.

Run No.	Wind Direction degrees	Original z_o m	Revised z_o m
13	10	0.23	0.05
141	40	0.07	0.07
67	55	0.07	0.03
30	70	0.12	0.02
165	100	0.38	0.14
101	105	0.42	0.39
163	110	0.10	0.10
176	115	0.17	0.16
149	125	0.11	0.06
139	136	0.35	0.11
133	140	0.40	0.14
162	180	0.80	0.35
155	180	0.90	0.40
142	210	0.10	0.02
91	275	0.48	0.33
121	335	0.26	0.26

direction according to Blackadar (personal communication). Second, some preliminary estimates suggest that the revised roughness lengths are more nearly consistent with the observations of standard deviations of u and v than the original roughness lengths.

In order to test Eq. (3.6), L_o was computed by assuming that the Richardson number computed from winds and temperatures at the lowest two levels equals z/L_o at the geometric mean of these two heights. Then, X was computed from Eq. (3.6) (Fig. 3.1), and plotted as function of height on log-log paper. This was compared with the observed variation of X with height. Since the observed and computed values of X could differ by a constant factor (depending on the ratio of revised to original roughness length), the theoretical line was shifted sideways until the best fit to the observed spectra is obtained. However, u-spectra and v-spectra were assumed to have the required 4/3 ratio. Figure 3.3 shows these fits. Clearly, Eq. (3.6) predicts the behavior of X with height quite well. Also, the assumption of isotropy is consistent with the observations.

There are only one or two exceptions in unstable air, where presumably the stability parameter is in error. Also, the vertical variation is not well matched on the stable side where ϕ_ϵ has been taken as $1 + 9 \, z/L_o$. Here one would not really expect surface layer approximations to be valid above a few meters because the turbulence structure fails to produce sufficient coupling between the lower and upper levels.

In order to remove the effect of the uncertain constant factor, ratios of the spectra at f = 1 at 120 m and 30 m were formed, and compared with ratios of these spectra computed from Eq. (3.6). The result is shown in Fig. 3.4. Here, the agreement is good.

In summary, it appears then that Eq. (3.6), which is based on the eddy energy equation without flux divergence, well accounts for the vertical variation of the spectra, although it does not explain their absolute values, unless the roughness lengths are adjusted.
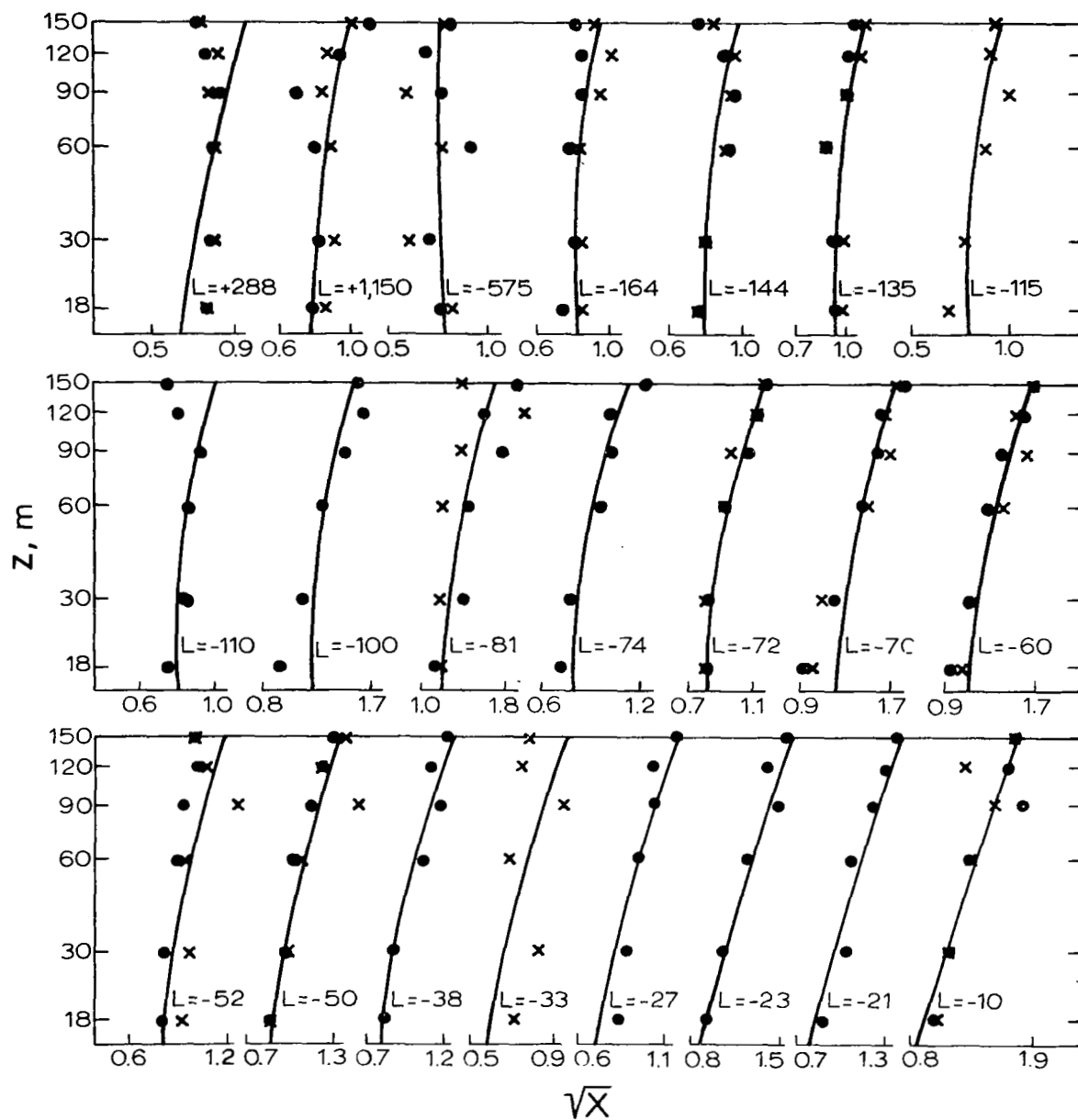
Figure 3.3 Fit of theoretical relation to observed relation between
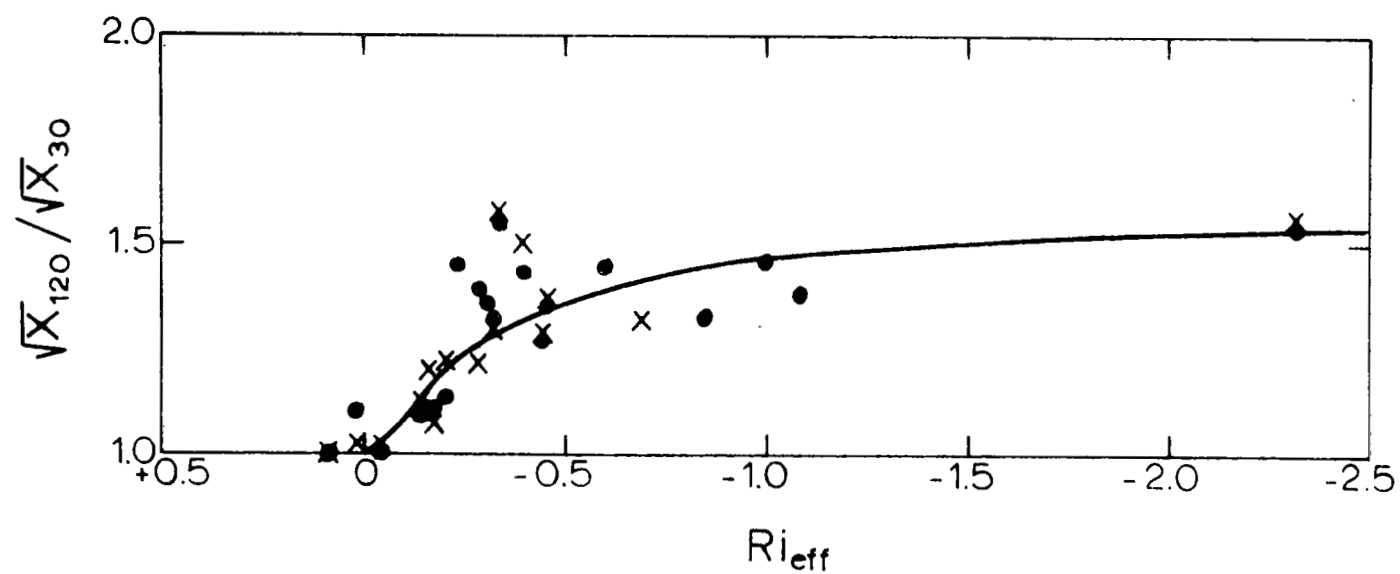$\sqrt{X}$ and height.

Figure 3.4   Ratio $\sqrt{X}$ at 120 m to $\sqrt{X}$ at 30 m as function of Ri_{eff}, theoretical (line) and observed (points). Dots, longitudinal and crosses, lateral velocity.

Given the adjusted roughness lengths, estimates of the inertial portion of the spectra in the inertial range can now be based on Eq. (3.7). First, the surface stress is obtained from a low-level wind and a stability correction in the usual manner. Then, the Richardson number computed from the lowest two winds is assumed to be equal to z/L_o; and X is found from Eq. (3.6) or Fig. 3.1. These estimates will be high for near neutral air for cases at high levels. Otherwise, such estimates appear to be valid up to 150 m in unstable air, and at lower levels in neutral and slightly stable air.

Since spectral estimation as discussed in this report has concentrated entirely on the inertial range, it is important to determine up to what frequency the -5/3 slope is valid. For a large number of runs values of $f = nz/V$ were estimated by eye up to which this simple power law could be assumed. Figure 3.5 shows this limiting value, denoted by f_b, plotted as function of height z and L. In addition to observations from Cape Kennedy, the graph contains data obtained at the 300-m tower at Obninsk by Volkovitskaya and Ivanov (1967).

It is clear that f_b increases with height, but more slowly than linearly, so that the limiting wavelength also increase upward. Further, the value of f_b is smaller in unstable than in stable air; but the detailed variation with L is rather irregular, or rather "noisy". With many more observations, a definite relation between average f_b and average stability could be established. Generally, the Russian observations are quite compatible with those obtained by Cape Kennedy.

In all but the most stable air, the inertial range seems to be valid up to wavelengths of about 100 m at z = 25 m; and to 200 m at z = 100 m. Sometimes, the -5/3 law seems to be valid to much longer wavelengths; the reason is not known.
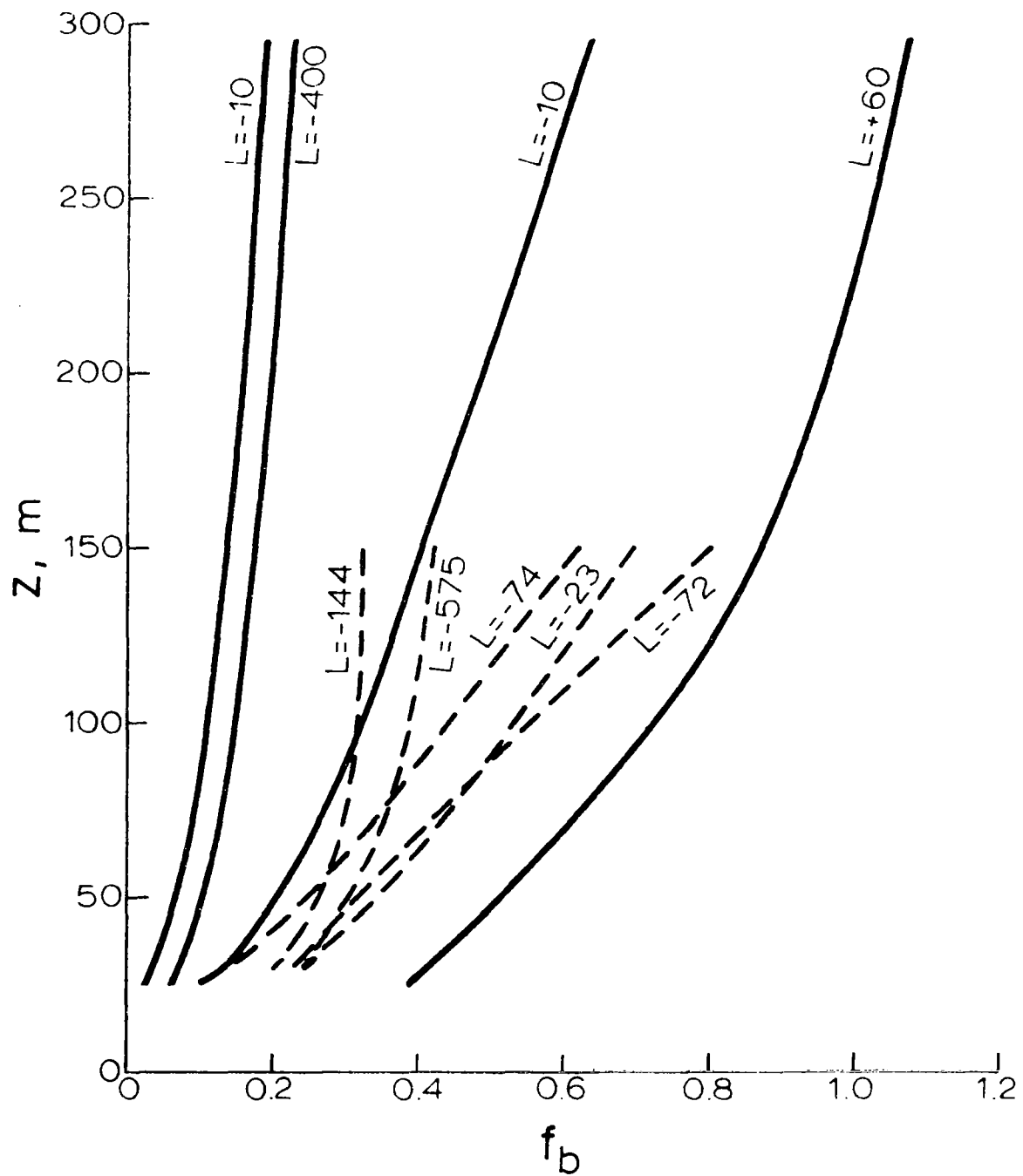
Figure 3.5   Lower limit of f = nz/V for validity of Kolmogorov law.
Solid lines, Russian data; broken lines, Cape Kennedy
observations.

References

Busch, N. E. and H. A. Panofsky, 1968: Recent spectra of atmospheric turbulence. Quart. J. R. Met. Soc., 94, 132-148.

Deardorff, J. W., 1968: Dependence of air-sea transfer coefficients on bulk stability. J. Geophys. Res., 73, 2549-2557.

Lumley, J. L. and H. A. Panofsky, 1964: *The Structure of Atmospheric Turbulence.* Interscience Monographs and Texts in Physics and Astronomy, v. XII, John Wiley & Sons, New York, 239 + xi pp.

Panofsky, H. A., 1962: The budget of turbulent energy in the lowest 100 meters. J. Geophys. Res., 67, 3161-3165.

Volkovitskaya, Z. I. and V. N. Ivanov, 1967: The low-frequency boundary of the inertial interval in the atmospheric boundary layer. Isv. Acad. Nauk SSSR, Atm. and Ocean. Phys., 3, 1053-1061.

IV. THE RELATION BETWEEN WIND COMPONENTS AT DIFFERENT HEIGHTS

Hans A. Panofsky

4.1 Theory

The spectral characteristics of the relationship between wind components at two heights are described by the cospectrum and the quadrature spectrum. We have already seen how these statistics were evaluated, between all pairs of levels available. However, so far, only like components at each pair of heights have been related to each other. From the cospectra and quadrature spectra (normalized by the spectra themselves), two new statistics, which are functions of the frequency n, can be computed; the coherence:

$$(4.1) \qquad coh(n) = c^2(n) + q^2(n)$$

and the eddy slope s:

$$(4.2) \qquad s(n) = [arc \ tan(q/c)/2\pi\Delta f$$

here, c and q (lower case) represent cospectra and quadrature spectra, respectively, normalized by the geometric mean of the corresponding spectra at the same frequency, at the two levels. Δf is defined by:

$$(4.3) \qquad \Delta f = n\Delta z/V$$

where n is the frequency, V the average wind in the layer analyzed, and Δz the separation between the upper and lower levels. If Taylor's "frozen wave" hypothesis is valid, Δf represents the ratio of vertical separation to horizontal wavelength.

The quantity s, the "eddy slope" is the ratio of space delay between a signal reaching the two heights, and Δz. Thus, a small value of s represents a nearly vertical eddy and vice versa.

It turns out that s(n) and coh(n) have simpler properties than c(n) and q(n). It is therefore suggested that the slope and the coherence be estimated as function of mean variables, and that q(n) and c(n) be computed by solving Eqs. (4.1) and (4.2) for them:

$$(4.4) \qquad q(n) = \sqrt{coh(n)} \; \sin(2\pi s\Delta f)$$

$$(4.5) \qquad c(n) = \sqrt{coh(n)} \; \cos(2\pi s\Delta f)$$

4.2 Analysis and estimation of coherence

As was suggested originally by Davenport (1961) there exists a kind of geometrical similarity in the lower atmosphere such that the coherence has relatively simple properties if analyzed as function of Δf rather than simply n. This means that an "eddy" with horizontal wavelength 1 km has the same sort of coherence when Δz is 100 m as an eddy of wavelength 500 m for a separation of 50 m.

Therefore, many graphs were constructed by computer, giving the relationship between coherence and Δf. An example is given in Fig. 4.1. Here, on the same graph coherences from many height combinations are analyzed. Apparently, the coherence is independent of height or of height interval Δz. However, comparison of many such graphs shows a variation with stability in the sense that, other things being equal, the coherence increases with decreasing stability. There also seem to be systematic differences between locations, which are not yet understood.

All of the coherence–Δf graphs have considerable, but unsystematic scatter. Within the apparently random variations of the individual points, simple exponential functions appear to fit the graphs. Therefore, the graphs were plotted on semilog paper, and straight lines were fitted by eye. Equations for these lines were then written in the form:

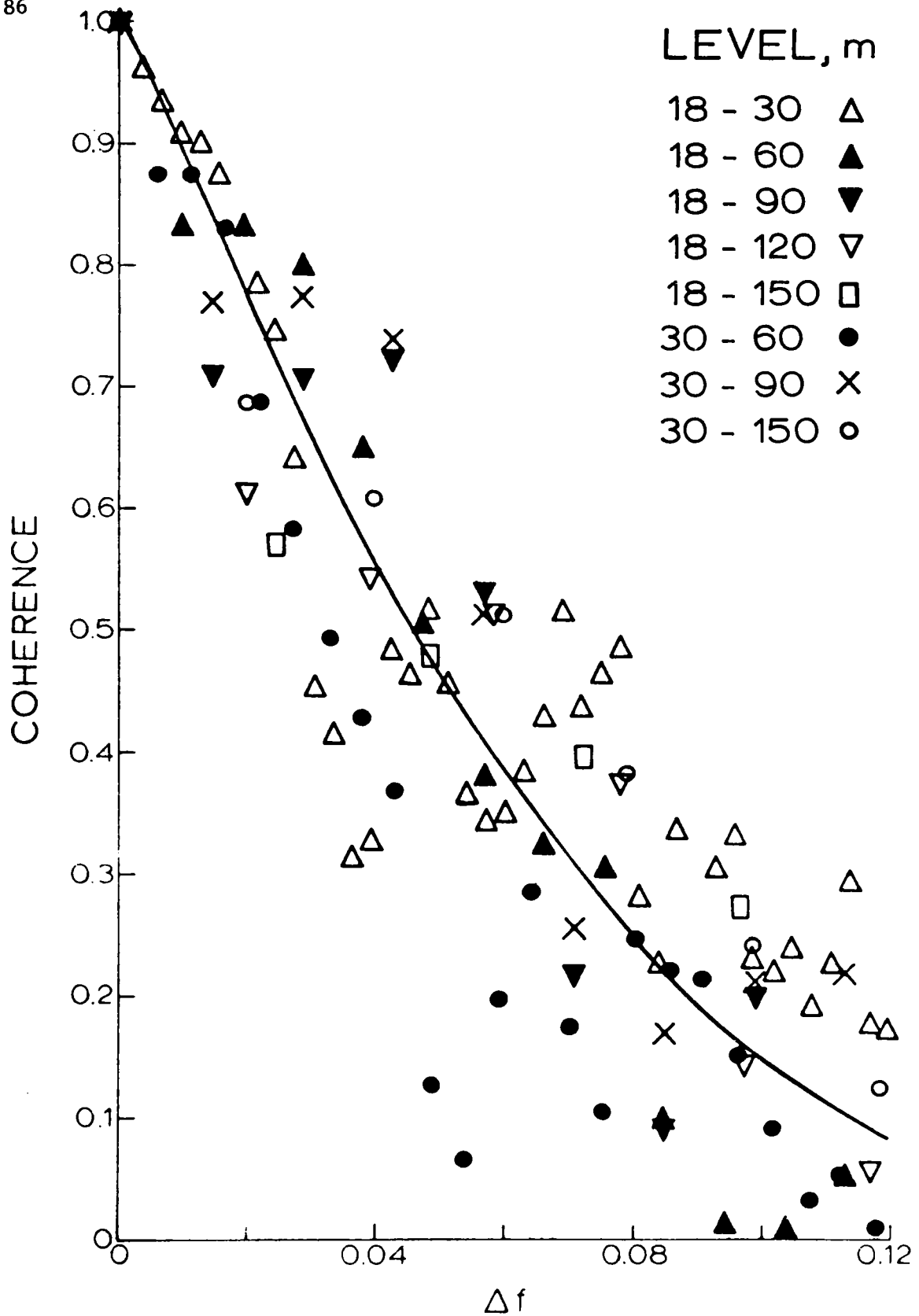$$(4.6) \qquad coh(n) = \exp(-.693\Delta f/\Delta f_{0.5})$$

Figure 4.1 Typical dependence of coherence on Δf.

The quantity $\Delta f_{0.5}$ is a constant for each line, which represents the value of Δf when the coherence drops to 0.5. This quantity is, presumably, a function of stability, and perhaps other factors such as terrain roughness or other topographic features. Of course, once $\Delta f_{0.5}$ is given, coherences can then be estimated from Eq. (4.6).

At first, the hypothesis was tested that coherence depends on the "power" of the wind profile, $d(\log V)/d(\log z)$, which is known to depend on stability, height and roughness. The results were disappointing, and are not given here.

Figures 4.2 and 4.3 give the relation between $f_{0.5}$ and Ri_{eff}, the effective Richardson number for the longitudinal and lateral wind components, respectively. As we noted earlier, this quantity is the Richardson number extrapolated linearly from a value computed close to the ground (see Chapter III). Observations from many sources are brought together in these figures. For the observations at the Brookhaven Laboratory, no satisfactory Richardson numbers were given; instead, the observations were classified according to the Brookhaven gustiness classification. This information was converted into Richardson number according to a recipe concocted by Pries (unpublished). Some fast-wind observations were assumed to be associated with zero Richardson number. Apparently, not all observations can be fitted by a single line. Two lines were drawn on each graph; one for the observations for Cape Kennedy, the other for all the remaining data. Why the coherences in unstable air at Cape Kennedy are significantly lower than elsewhere (as indicated by the graphs) is not clear. One might suspect an error of computation, but none was found in spite of thorough checking. In stable and neutral air, the agreement between sites is fairly good; coherence effectively disappears for a Richardson number between 0.25 and 0.50, in agreement with other estimates of the "critical" Richardson number.

In general, coherences of u- and v-components are not greatly different from each other, with slightly larger coherences indicated for lateral components in unstable air. Altogether, then, Figs. 4.2 and 4.3 along with Eq. (4.6) permit estimation of coherences at the locations
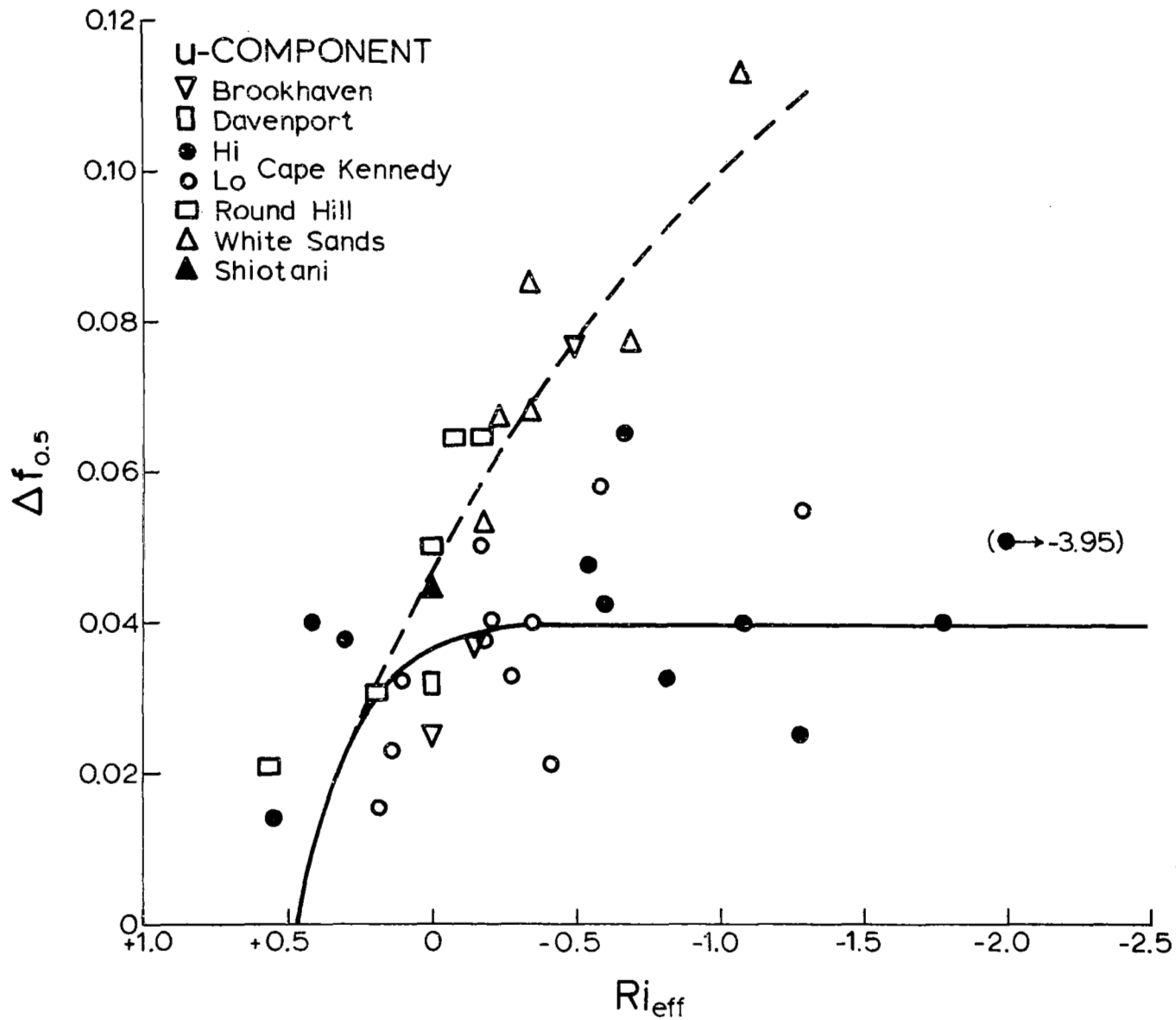
Figure 4.2 Dependence of $f_{0.5}$ on Ri_{eff} for the u-component. Solid line, fit to Cape Kennedy site; broken line, fit to sites other than Cape Kennedy.
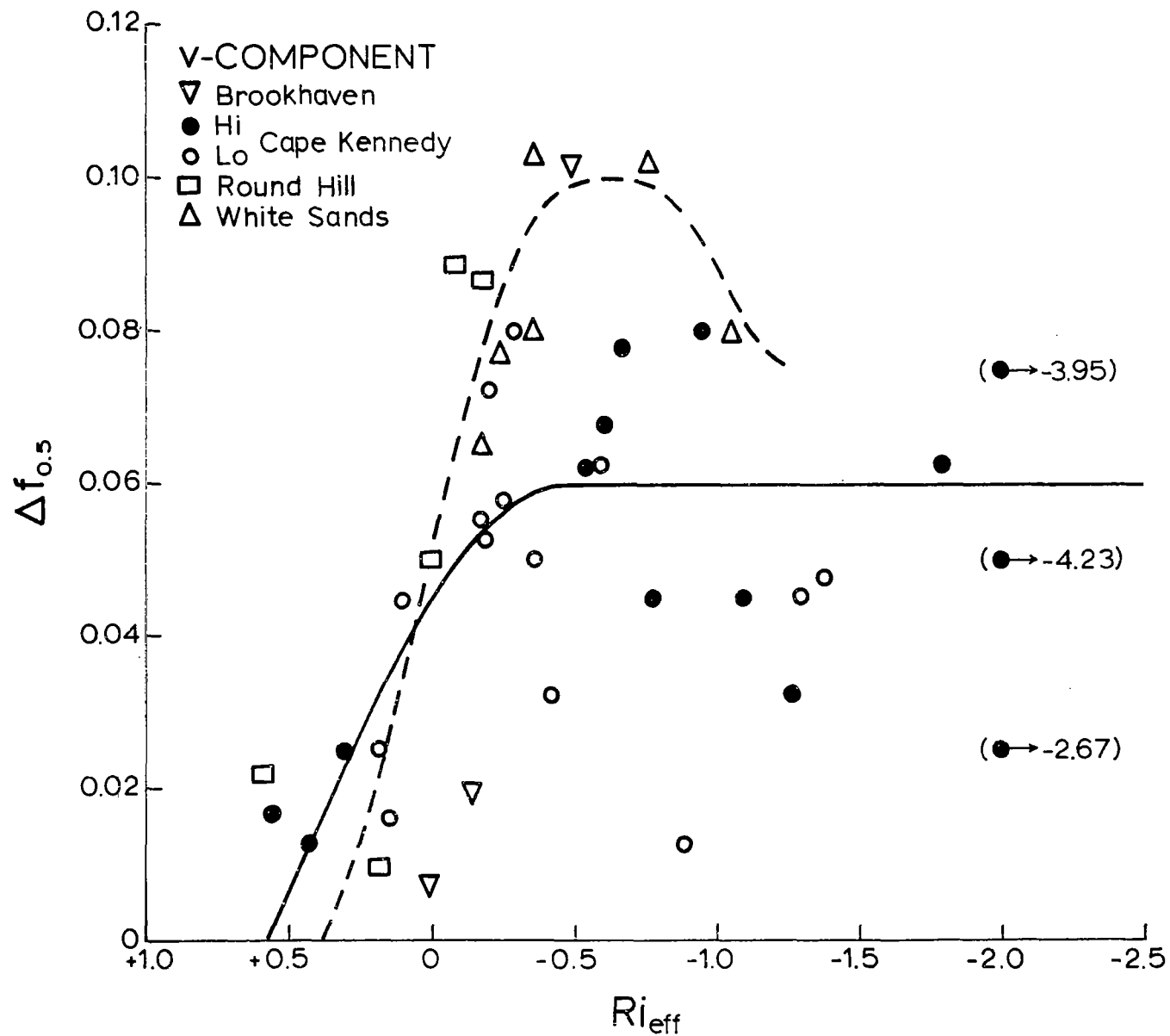
Figure 4.3 Dependence of $f_{0.5}$ on Ri_{eff} for the v-component. Solid line, fit to Cape Kennedy site; broken line, fit to sites other than Cape Kennedy.

included in the graphs. As input, one would need two winds and two
temperatures below 30 m or so. From these, Richardson numbers would be
computed and vertically extrapolated to the geometric mean of two heights
in question; the mean wind in the layer between these heights required
in the computation of Δf can be estimated with sufficient accuracy by
linear extrapolation or interpolation of the two low-level winds on a
graph with a logarithmic height scale. Probably almost equally good
estimates of $\Delta f_{0.5}$ are possible by use of Pasquill's stability classes
(Pasquill, 1962) instead of Richardson numbers.

Finally, all the coherence graphs indicated a great deal of
scatter, suggesting that the coherence estimates are not very precise.
In fact, for $\Delta f > 0.12$, the coherence can be regarded as negligible.

4.3 Analysis and estimation of slope s

A program was developed which fitted parabolae of the form:

$$(4.7) \qquad y = 1 - ax + bx^2$$

to the cospectra and

$$(4.8) \qquad y = cx - dx^2$$

to the quadrature spectra, where a, b, c and d are constants. Some of
the results were machine-plotted and appeared to fit the observations
reasonably well. From these parabolae, slopes were computed at $f = 0.05$
and $f = 0.10$.

First, the slopes at $f = 0.05$ were analyzed with respect to
height and Richardson number. Only systematic changes with height were
found. Thus, for the u-components, the average slope s was 0.7 when
all observations were at or below 90 m. For all observations at or above
that level, the average was 0.5.

The slopes for the v-components are much larger than those of
the u-components not only at Cape Kennedy, but also at three other sites.

The average slope from combinations of v-components at 18 m with v-components at 30 m and 60 m is 1.7; slopes between 30 m and 90 m average 1.4, but slopes involving v-components only at 90m and higher levels average only 0.55. At present, the difference between the slopes in the two lower layers can hardly be judged significant; but the change to lower values above 90 m certainly is. Perhaps, for the time being, it would be justified to use s = 0.7 and s = 1.5 for the u- and v-components, respectively, below 90 m, and slopes of 0.5 above that level for both components.

The difference between slopes at f = 0.10 and at 0.05 was also analyzed as function of effective Richardson number. The result, with some observations from White Sands added, is given in Fig. 4.4. Each point represents an average in a given class of Richardson numbers. Except for some u-components during stable periods, there is no significant difference at the two frequencies. Therefore, for the time being, it is recommended to assume that the slopes s for u and v are independent of frequency.

References

Davenport, A. G., 1961: The spectrum of horizontal gustiness near the ground in high winds. Quart. J. R. Met. Soc., 87, 194–211.

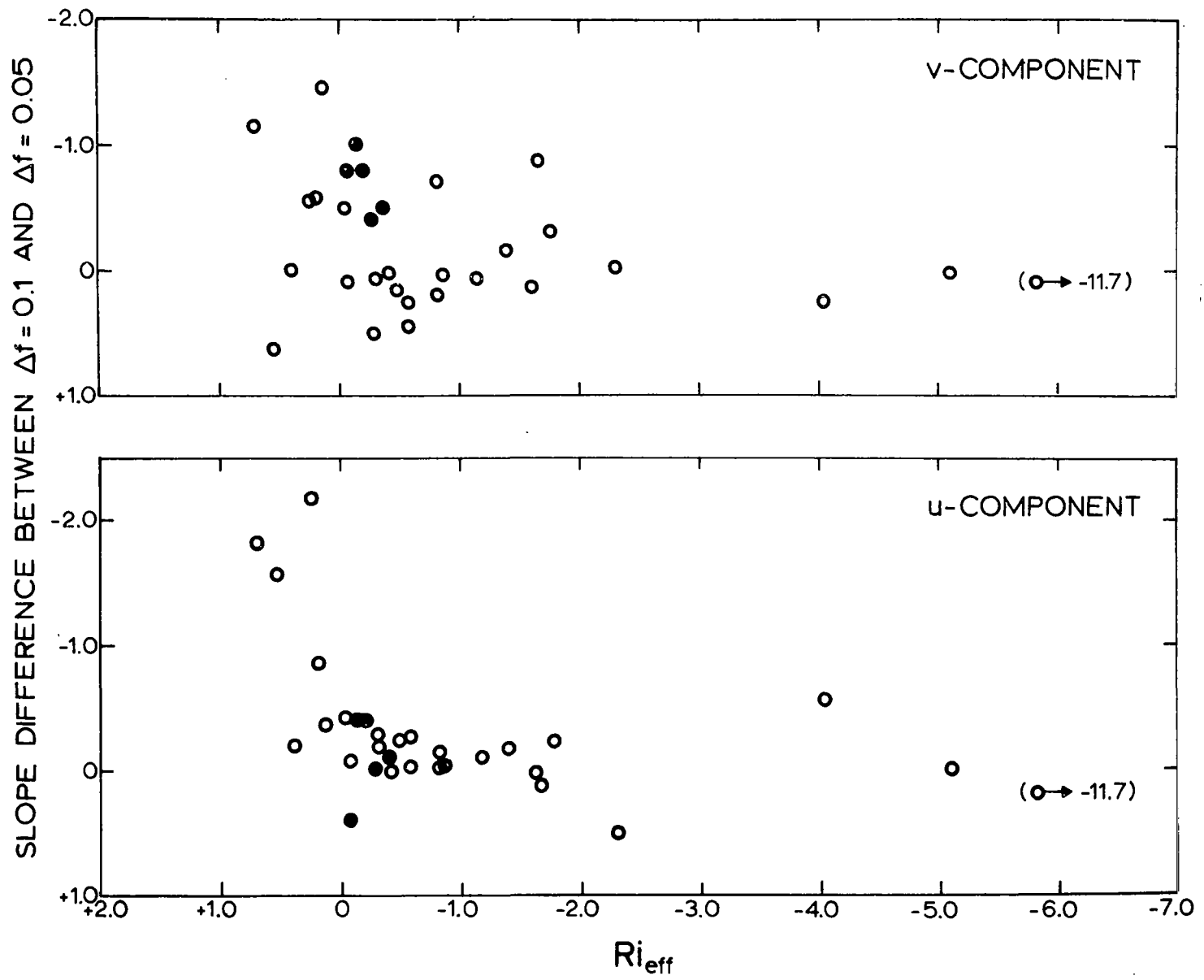Pasquill, F., 1962: *Atmospheric Diffusion*. D. Van Nostrand, Princeton, 297 pp.

Figure 4.4 Slope difference between f = 0.1 and f = 0.05 as function of Ri_{eff}.